NASA CONTRACTOR REPORT 182021

AN EQUIVALENT DOMAIN INTEGRAL METHOD FOR THREE-DIMENSIONAL MIXED-MODE FRACTURE PROBLEMS

K. N. Shivakumar and I. S. Raju
Analytical Services and Materials, Inc.
Hampton, VA

Contract NASI-18599
AUGUST 1991

National Aeronautics and Space Administration

LANGLEY RESEARCH CENTER
Hampton, Virginia 23665-5225

AN EQUIVALENT DOMAIN INTEGRAL METHOD FOR THREE-DIMENSIONAL MIXED-MODE FRACTURE PROBLEMS

K. N. Shivakumar and I. S. Raju
Analytical Services and Materials, Inc.
Hampton, VA

ABSTRACT

A general formulation of the equivalent domain integral (EDI) method for mixed-mode fracture problems in cracked solids is presented. The method is discussed in the context of a 3-D finite element analysis. The $J-$integral consists of two parts: the volume integral of the crack front potential over a torus enclosing the crack front and the crack surface integral due to the crack front potential plus the crack-face loading. In mixed-mode crack problems the total J-integral is split into J_I, J_{II}, and J_{III} representing the severity of the crack front in three modes of deformations. The direct and decomposition methods are used to separate the modes. These two methods were applied to several mixed-mode fracture problems in isotropic materials. Several pure and mixed-mode fracture problems were analyzed and results found to agree well with those available in the literature. The method lends itself to be used as a post-processing subroutine in a general purpose finite-element program.

INTRODUCTION

Several numerical techniques, in conjunction with finite-element (F-E) analyses, have been developed to calculate fracture mechanics parameters (stress-intensity factor K, strain energy release rate G, and J-integral). Three of these techniques are: (1) the virtual crack extension (VCE) method [1-4], (2) the virtual crack closure technique (VCCT) [5-8], and (3) the J-integral method [9-12]. The VCCT method is simple and accurate but can be applied only to linear elastic problems. In contrast, the VCE and J-integral methods can be applied to both linear and nonlinear problems. These methods are best demonstrated for pure mode problems or for calculating the total crack driving forces (G or J). Application of these methods to mixed-mode fracture problems is complex. The VCE

method involves a physical extension of the crack front by a small amount. Selection of the amount of crack extension is arbitrary and can introduce errors in inelastic problems. Further, both VCCT and VCE methods require a F-E mesh that is nearly normal to the crack front. Except for some simple cases, generating such customized F-E models for irregular-shaped cracks is difficult and time consuming, if not impossible. Furthermore, such detailed modeling may not improve the global accuracy of the boundary value solution. Therefore, pursuit of methods that do not have these limitations continues.

The J-integral method is very attractive, particularly for nonlinear material problems. With the original J-integral equation by Rice [9], Cherepanov [10,12], and Eshelby [11] for two-dimensional (2-D) problems as the starting point, several crack tip integrals were developed to include body forces due to thermal and magnetic fields and unloading effects in elastic-plastic problems [13-18]. For 2-D problems, the crack tip integrals are written as the sum of a remote line integral and an area integral around the crack tip. For 3-D problems, the J-integral is the sum of a remote surface integral and a volume integral around the crack front. These integral formulations suffer from a common drawback in that they require the evaluation of surface integrals which include singular terms. The evaluation of these surface integrals, although possible, is very unwieldy in F-E analyses.

The J-integral formulation has been modified into a domain integral form [19-23] after de Lorenzi [24,25] introduced a S-function concept to define the virtual crack extension in 3-D cracked solids. In this method, the surface integrals for 3-D problems can be transformed into integrals over a domain or volume and, hence, the name equivalent domain integral (EDI). The EDI formulation is computationally very appealing and efficient.

Recently, Nikishkov and Atluri [20] presented an EDI formulation for cracked 3-D solids. To simulate the singularities at the crack front, they used quarter-point singularity elements. While they present the EDI formulation in a comprehensive manner, some details of the formulation need additional explanation. Also the formulation of reference 20 may not be general enough for problems where crack faces are subjected to external loading. The first objective of this paper is to present a general formulation of the EDI method for the calculation of J-integral under mixed-mode loading conditions.

Most investigators use collapsed quarter-point singularity elements at the crack front to simulate the crack front singularity with a polar arrangement of elements around the crack front. This type of mesh may be suitable but not convenient, particularly, for crack extension studies. Furthermore, in the plastic range the quarter-point singular element produces a $1/r$ type singular strain field, which is valid only for elastic-perfectly-plastic material. Therefore, the second objective of this paper is to study the accuracy of the results when non-singular elements with a rectilinear arrangement of elements are used at the crack front.

First the EDI formulation for general mixed-mode fracture problems in elastic, elastic-plastic, and anisotropic materials is presented. Next, the validity of the formulation is studied by applying it to several linear elastic and isotropic mixed-mode fracture problems. Numerical implementation of the EDI method for 20-noded and 8-noded, 3-D isoparametric elements is presented in the appendix. Several differences between the present formulation and those in the literature are highlighted.

CRACK FRONT AND DOMAIN INTEGRALS

The J-integral was introduced by Rice [9], Cherepanov [10], and Eshelby [11] to define the strength of the stress-strain field in nonlinear elastic 2-D crack problems. The J-integral was shown to be path-independent for nonlinear elastic and power-law hardening elastic-plastic materials. This path independence can be explained based on one singular point (crack tip) inside a closed contour in a singly connected domain.

In 3-D crack problems, the crack front forms a line singularity and the strength of the singularity (K or J) could be varying all along the crack front. Therefore, the path independency is valid in a global sense, that is the total (or average) strength of the singularity of the complete crack front is independent of the surface enclosing it. However, at a point on the crack front, the path independency is valid only over a small region around the crack front due to interacting singular fields at neighboring points on the crack front.

Consider a small tube of radius ϵ around a segment of crack front of length Δ as shown in Figure 1(a) such that the limit of Δ and $\frac{\epsilon}{\Delta}$ tends to zero. The

local J-integral, also referred to as the crack front integral, over the surface A_ϵ is defined as (see Fig. 1(a)) [12,20]

$$\int_\Delta J_{x_k}\, dx_3 \;=\; \lim_{\substack{\epsilon \to 0 \\ \Delta \to 0}} \int [W\, n_k \;-\; \sigma_{ij} \frac{\partial u_i}{\partial x_k}\, n_j]\; dA \tag{1}$$

In Equation (1), W is the stress-work density, σ_{ij} is the stress tensor, u_i is the displacement vector, and n_k is the k^{th} directional component of the unit normal vector on the closed surface A_ϵ. The indices i and j take the values 1, 2, and 3, and k takes the values 1 and 2. Thus the local value of J_{x_k} is the total energy flux leaving the closed surface A_ϵ per unit crack front length in the k^{th} direction. J_{x_k} can be defined in any coordinate system, but the local crack front coordinate system x_1, x_2, and x_3 is convenient for crack-extension studies. Note that the axes x_1 and x_3 are in the crack plane and are normal and tangential to the crack front, respectively, while x_2 is normal to the crack plane.

The complete surface integral, in terms of surfaces identified in the Figure 1(a), is written as (henceforth the limits are dropped for convenience of presentation)

$$\int_\Delta J_{x_k}\, dx_3 \;=\; \int_{A_\epsilon} Q\, dA \;+\; \int_{A_{\epsilon_1}+A_{\epsilon_2}} Q\, dA \;+\; \int_{A_{\epsilon_{ct}}+A_{\epsilon_{cb}}} Q\, dA \tag{2}$$

where

$$Q \;=\; [W\, n_k \;-\; \sigma_{ij} \frac{\partial u_i}{\partial x_k}\, n_j] \tag{3}$$

$$W \;=\; \int_0^{\epsilon_{ij}} \sigma_{ij}\, d\epsilon_{ij} \tag{4}$$

In Equation (2), $A_{\epsilon 1}$ and $A_{\epsilon 2}$ are cross-sectional areas of the tube at O_1 and O_2, respectively. The subscripts ct and cb represent top and bottom crack surfaces, respectively. The stress-work density in Equation (4) is calculated over the complete strain path. The total strain tensor ϵ_{ij} includes elastic, plastic, and thermal components. For linear elastic problems, $W = \frac{(\sigma_{ij}\epsilon_{ij})}{2}$. Note that Equation (2) involves only stress, displacement and strain fields but no material properties.

However, to calculate stresses from strains the appropriate constitutive relationships (isotropic or anisotropic) must be used. Thus Equation (2) is applicable for general thermo-elastic-plastic and anisotropic material problems.

Fracture modes in a 3-D cracked solid can be represented by three modes: opening (mode I), shearing (mode II), and tearing (mode III) modes. The corresponding three modes of the J-integral are J_I, J_{II}, and J_{III}. In Equation (1) or (2), J_{x1} and J_{x2} represent the total J-integral ($J_I + J_{II} + J_{III}$) and the product integral ($-2\sqrt{J_I \cdot J_{II}}$), respectively [12, 19, 20]. Since the meaning of J_{x3} integral is not clear for crack problems, it is not defined by Equations (1) or (2). However, the mode III integral is separately defined as [20]

$$\int_{\Delta} J_{III}\, dx_3 = \lim_{\substack{\epsilon \to 0 \\ \Delta \to 0}} \left[\int_{A_\epsilon} Q_3\, dA + \int_{A_{\epsilon 1} + A_{\epsilon 2}} Q_3\, dA + \int_{A_{\epsilon ct} + A_{\epsilon cb}} Q_3\, dA \right] \tag{5}$$

where

$$Q_3 = W^{III}\, n_1 - \sigma_{3j} \frac{\partial u_3}{\partial x_1}\, n_j \tag{6}$$

$$W^{III} = \int_0^{\epsilon_{3j}} \sigma_{3j}\, d\epsilon_{3j} \tag{7}$$

The indices i and j take values 1, 2, and 3. Equations (2) through (7) completely define all three J-integrals. As previously mentioned, the evaluation of surface integrals, Equations (2) and (5), is tedious and could introduce errors due to numerical integration of singular terms. Therefore, an alternate form of evaluating the above surface integrals called the Equivalent Domain Integrals (EDI) is presented in the next section.

Equivalent Domain Integral

Consider two tubular surfaces A_ϵ and A spanning between two points O_1 and O_2 on the crack front (see Fig. 1(b)). The tube A is arbitrary and encloses the tube A_ϵ on which the J-integral is evaluated. The surface integrals (Eqs. (2) and

(5)) on A_ϵ are converted into volume integrals by mathematical manipulations. First, the right hand side of Equations (2) and (5) are multiplied by unity. Next, from the resulting right hand side of the equation, subtract the product of the same integral over the surface A and zero, as shown below.

$$\begin{aligned}\int_\Delta J_{x_k}\, dx_3 \;=\; & 1\cdot\int_{A_\epsilon} Q\, dA \;+\; 1\cdot\int_{A_{\epsilon 1}+A_{\epsilon 2}} Q\, dA \\ & +\; 1\cdot\int_{A_{\epsilon ct}+A_{\epsilon cb}} Q\, dA \;-\; 0\cdot\int_A Q\, dA\end{aligned} \tag{8}$$

$$\begin{aligned}\int_\Delta J_{III}\, dx_3 \;=\; & 1\cdot\int_{A_\epsilon} Q_3\, dA \;+\; 1\cdot\int_{A_{\epsilon 1}+A_{\epsilon 2}} Q_3\, dA \\ & +\; 1\cdot\int_{A_{\epsilon ct}+A_{\epsilon cb}} Q_3\, dA \;-\; 0\cdot\int_A Q_3\, dA\end{aligned} \tag{9}$$

Note that, Equations (8) and (9) assume a unit extension of the crack front segment in the x_1-direction. Instead, if an arbitrary (nonuniform) virtual extension of the crack front is made, Equations (8) and (9) need to be modified to account for this variation. Therefore, an arbitrary but continuous function $S(x_1, x_2, x_3)$ is introduced [19, 20, 23] that has the property $S(x_1, x_2, x_3) = 0$ on the surface A and $S(x_1, x_2, x_3) = S(x_3)$ on the surface A_ϵ. Using the S-function, Equations (8) and (9) are rewritten as follows.

$$\begin{aligned}\int_\Delta J_{x_k}\, S\, dx_3 \;=\; & \int_{A_\epsilon} Q\, S\, dA \;+\; \int_{A_{\epsilon 1}\,+\,A_{\epsilon 2}} Q\, S\, dA \\ & +\; \int_{A_{\epsilon ct}\,+\,A_{\epsilon cb}} Q\, S\, dA \;-\; \int_A Q\, S\, dA\end{aligned} \tag{8a}$$

$$\begin{aligned}\int_\Delta J_{III}\, S\, dx_3 \;=\; & \int_{A_\epsilon} Q_3\, S\, dA \;+\; \int_{A_{\epsilon 1}\,+\,A_{\epsilon 2}} Q_3\, S\, dA \\ & +\; \int_{A_{\epsilon ct}\,+\,A_{\epsilon cb}} Q_3\, S\, dA \;-\; \int_A Q_3\, S\, dA\end{aligned} \tag{9a}$$

As previously mentioned, Δ is small ($\lim\ \Delta \to 0$) and, hence, J_{x_k} is assumed to be constant over the crack front segment length Δ. Then, Equations (8a) and (9a) are simplified to

$$J_{x_k} \cdot f = \int_{A_\epsilon} Q\,S\,dA + \int_{A_{\epsilon 1} + A_{\epsilon 2}} Q\,S\,dA + \int_{A_{\epsilon ct} + A_{\epsilon cb}} Q\,S\,dA - \int_{A} Q\,S\,dA \tag{10}$$

$$J_{III} \cdot f = \int_{A_\epsilon} Q_3\,S\,dA + \int_{A_{\epsilon 1} + A_{\epsilon 2}} Q_3\,S\,dA + \int_{A_{\epsilon ct} + A_{\epsilon cb}} Q_3\,S\,dA - \int_{A} Q_3\,S\,dA \tag{11}$$

where

$$f = \int_{O_1}^{O_2} S(x_3)\,dx_3 \tag{12}$$

The parameter f is equivalent to the new crack surface area created by translating the crack front by $S(x_3)$ in the x_1- direction. Evaluation of f in Equation (12) and the choice of the S-function will be discussed later. Equations (10) and (11) were further simplified by selecting the S-function such that the function has zero values at two end surfaces (O_1 and O_2) of the tubes A_ϵ and A and non-zero between these two end faces. With this choice, the second surface integrals in Equations (10) and (11) become identically zero.

Now the integrals on the crack faces between the inner (A_ϵ) and outer (A) tubes are added and subtracted from the right hand sides of Equations (10) and (11). This manipulation is performed to obtain the integrals on a closed surface that encloses a volume. After some elementary algebraic operations, Equations (10) and (11) is rewritten as follows

$$J_{x_k} \cdot f = -\int_{A + (A - A_\epsilon)_{ct} + A_\epsilon + (A_\epsilon - A)_{cb}} Q\,S\,dA + \int_{(A - A_\epsilon)_{ct}} Q\,S\,dA + \int_{(A_\epsilon - A)_{cb}} Q\,S\,dA + \int_{A_{\epsilon ct} + A_{\epsilon cb}} Q\,dA \tag{13}$$

$$J_{III} \cdot f = -\int_{A + (A - A_\epsilon)_{ct} + A_\epsilon + (A_\epsilon - A)_{cb}} Q_3 \, S \, dA + \int_{(A - A_\epsilon)_{ct}} Q_3 \, S \, dA + \int_{(A_\epsilon - A)_{cb}} Q_3 \, S \, dA + \int_{A_{\epsilon ct} + A_{\epsilon cb}} Q_3 \, dA \qquad (14)$$

The first term in Equations (13) and (14) is negative because the direction of integration on the inner surface of the tube (A_ϵ) is reversed. In Equations (13) and (14), $(A - A_\epsilon)_{ct}$ and $(A_\epsilon - A)_{cb}$ are the top and bottom crack surface areas between the two tubes A and A_ϵ. The first term in Equations (13) and (14) encloses the volume between the two tubes A and A_ϵ, which is represented as $(V - V_\epsilon)$. The rest of the terms in the right-hand sides of Equations (13) and (14) are integrals on the crack faces. Hence, J_{x_k} and J_{III} are expressed as the sum of domain and crack surface integrals as follows

$$J_{x_k} \cdot f = (J_{x_k} \cdot f)_{domain} + (J_{x_k} \cdot f)_{crack faces} \qquad (15)$$

$$J_{III} \cdot f = (J_{III} \cdot f)_{domain} + (J_{III} \cdot f)_{crack faces} \qquad (16)$$

Reference 20 obtained similar equations but did not include the crack face integrals. However, as will be shown later, for special cases the crack-face integrals vanish and the complete J-integral is given by the domain part of Equations (15) and (16).

Domain integral.- Invoking Green's divergence theorem, the closed surface integral of Equations (13) and (14) are written as a domain integral as follows

$$(J_{x_k} \cdot f)_{domain} = -\int Q \, S \, dA$$

$$= -\int [W n_k - \sigma_{ij} \frac{\partial u_i}{\partial x_k} n_j] \, S \, dA \qquad (17)$$

$$= -\int_{(V - V_\epsilon)} [\frac{\partial (WS)}{\partial x_k} - \frac{\partial}{\partial x_j}(\sigma_{ij} \frac{\partial u_i}{\partial x_k} S)] \, dV$$

Hence, the domain integral is

$$(J_{x_k} \cdot f)_{domain} = -\int_{(V-V_\epsilon)} [\, W \frac{\partial S}{\partial x_k} - \sigma_{ij} \frac{\partial u_i}{\partial x_k} \frac{\partial S}{\partial x_j} \,]\, dV - \int_{(V-V_\epsilon)} [\, \frac{\partial W}{\partial x_k} - \sigma_{ij} \frac{\partial \epsilon_{ij}}{\partial x_k} \,]\, S\, dV \tag{18}$$

Similarly one has

$$(J_{III} \cdot f)_{domain} = -\int_{(V-V_\epsilon)} [\, W^{III} \frac{\partial S}{\partial x_1} - \sigma_{3j} \frac{\partial u_3}{\partial x_1} \frac{\partial S}{\partial x_j} \,]\, dV - \int_{(V-V_\epsilon)} [\, \frac{\partial W^{III}}{\partial x_1} - \sigma_{3j} \frac{\partial}{\partial x_1} (\frac{\partial u_3}{\partial x_j})] \, S\, dV \tag{19}$$

In deriving Equations (18) and (19), the equations of equilibrium

$$\frac{\partial \sigma_{ij}}{\partial x_j} = 0$$

and the small deformation strain-displacement relationships

$$\epsilon_{ij} = \frac{1}{2} (\frac{\partial u_i}{\partial x_j} + \frac{\partial u_j}{\partial x_i})$$

were used.

In conventional finite element analysis, the equations of equilibrium are not satisfied point wise in the domain that is modeled. Numerical experimentation showed that the differences between including and not including the terms involving the equations of equilibrium are of the order of 10^{-3} to 10^{-4} of the integral values for several problems. Therefore, in writing Equations (18) and (19) the equations of equilibrium are assumed to be satisfied exactly.

The terms in brackets in the second integral in Equations (18) and (19) are point wise equal to zero for a linear elastic material. These terms, however, are non-zero in elastic-plastic and thermal problems. Since the present formulation is

for general thermo-elastic-plastic problems, such simplifications are not incorporated.

The domain integral Equation (18) is rewritten in a matrix form as

$$
\begin{aligned}
(J_{x_k} \cdot f)_{domain} &= -\int_{(V-V_\epsilon)} [\, W \frac{\partial S}{\partial x_k} - \{ u'_{x_k} \}^T [\underline{\sigma}] \{ S' \}\,] \, dV \\
&\quad - \int_{(V-V_\epsilon)} [\, \frac{\partial W}{\partial x_k} - \{ \sigma \}^T \{ \epsilon'_{x_k} \}\,] \, S \; dV
\end{aligned} \tag{20}
$$

where

$$
\{\sigma\}^T = \{\, \sigma_{11} \quad \sigma_{22} \quad \sigma_{33} \quad \sigma_{12} \quad \sigma_{23} \quad \sigma_{31} \,\}
$$

$$
\{\epsilon'_{x_k}\}^T = \{\, \frac{\partial \epsilon_{11}}{\partial x_k} \quad \frac{\partial \epsilon_{22}}{\partial x_k} \quad \frac{\partial \epsilon_{33}}{\partial x_k} \quad 2\frac{\partial \epsilon_{12}}{\partial x_k} \quad 2\frac{\partial \epsilon_{23}}{\partial x_k} \quad 2\frac{\partial \epsilon_{31}}{\partial x_k} \,\}
$$

$$
\{u'_{x_k}\}^T = \{\, \frac{\partial u_1}{\partial x_k} \quad \frac{\partial u_2}{\partial x_k} \quad \frac{\partial u_3}{\partial x_k} \,\}
$$

$$
[\,\underline{\sigma}\,] = \begin{bmatrix} \sigma_{11} & \sigma_{12} & \sigma_{31} \\ \sigma_{12} & \sigma_{22} & \sigma_{23} \\ \sigma_{31} & \sigma_{23} & \sigma_{33} \end{bmatrix}
$$

$$
\{\, S' \,\}^T = \{\, \frac{\partial S}{\partial x_1} \quad \frac{\partial S}{\partial x_2} \quad \frac{\partial S}{\partial x_3} \,\} \tag{21}
$$

and the stress-work density W is

$$
W = \int_0^{\epsilon} [\, \sigma_{11} d\epsilon_{11} + \sigma_{22} d\epsilon_{22} + \sigma_{33} d\epsilon_{33} + 2\sigma_{12} d\epsilon_{12} + 2\sigma_{23} d\epsilon_{23} + 2\sigma_{31} d\epsilon_{31} \,].
$$

Similarly, the mode III integral Equation (19) is written as

$$
\begin{aligned}
(J_{III} \cdot f)_{domain} &= -\int_{(V-V_\epsilon)} [\, W^{III} \frac{\partial S}{\partial x_k} - \frac{\partial u_3}{\partial x_1} \{ \sigma_3 \}^T \{ S' \}\,] \, dV \\
&\quad - \int_{(V-V_\epsilon)} [\, \frac{\partial W^{III}}{\partial x_1} - \{ \sigma_3 \}^T \{ u''_3 \}\,] \, S \; dV
\end{aligned} \tag{22}
$$

where

$$\{\sigma_3\}^T = \{\sigma_{31} \quad \sigma_{32} \quad \sigma_{33}\}$$

$$\{u_3''\}^T = \{\frac{\partial^2 u_3}{\partial x_1{}^2} \quad \frac{\partial^2 u_3}{\partial x_1 \partial x_2} \quad \frac{\partial^2 u_3}{\partial x_1 \partial x_3}\} \tag{23}$$

and

$$W^{III} = \int_0^{\epsilon} [\, \sigma_{33} d\epsilon_{33} + \sigma_{31} d\epsilon_{31} + \sigma_{32} d\epsilon_{32} \,].$$

The numerical implementation of Equations (20) and (22) in a finite-element analysis with isoparametric elements is presented in the Appendix.

The integral J_{x_1} in Equation (20) for the linear elastic case is equivalent to the total strain-energy release rate calculated by the virtual crack extension method [1-4, 13, 24, 25].

Crack-face integrals.- The crack-face integrals in Equations (13) and (14) are

$$(J_{x_k} \cdot f)_{crackface} = \int_{(A-A_\epsilon)_{ct}} Q\, S\, dA + \int_{(A_\epsilon - A)_{cb}} Q\, S\, dA + \int_{A_{\epsilon ct} + A_{\epsilon cb}} Q\, dA \tag{24}$$

and

$$(J_{III} \cdot f)_{crackface} = \int_{(A-A_\epsilon)_{ct}} Q_3\, S\, dA + \int_{(A_\epsilon - A)_{cb}} Q_3\, S\, dA + \int_{A_{\epsilon ct} + A_{\epsilon cb}} Q_3\, dA \tag{25}$$

When the terms Q (Eq. (3)) and Q_3 (Eq. (6)) are zero on the crack faces, obviously, the integrals in Equations (24) and (25) vanish. On the crack faces, n_1 and n_3 are always zero, while $n_2 = -1$ on the top face (ct) and $n_2 = 1$ on the bottom face (cb). Imposition of these conditions in Equations (3) and (6), results in the following.

For $k = 1$

$$(Q)_{crackface} = -\sigma_{i2}\frac{\partial u_i}{\partial x_1}n_2$$

$$(Q_3)_{crackface} = -\sigma_{32}\frac{\partial u_3}{\partial x_1}n_2 \tag{26}$$

For $k = 2$

$$(Q)_{crackface} = Wn_2 - \sigma_{i2}\frac{\partial u_i}{\partial x_2}n_2 \tag{27}$$

Note that for $k = 2$, Q_3 is zero.

Thus for traction free crack faces the terms $(J_{x_1})_{crackface}$ and $(J_{III})_{crackface}$ vanish. In contrast, the term $(J_{x_2})_{crackface}$ is no longer zero. As noted in reference 23, the $(J_{x_2})_{crackface}$ is zero only for pure mode-I fracture problems or for a singular stress field alone. However, in any finite size cracked body the stress field consists of both singular and non-singular terms and, hence, the $(J_{x_2})_{crackface}$ integral is not zero and cannot be neglected. The numerical evaluation of crack-face integrals involve the computation of singular integral terms, which are computationally cumbersome and the source of errors [23].

Separation of Modes in Mixed-Mode Problems

There are three modes of deformations in a cracked body, namely, the opening mode (Mode I), the shearing mode (Mode II), and the tearing mode (Mode III). The direct and decomposition methods are used to separate the mixed-mode fracture mechanics parameters into the three individual modes.

Direct method.- The three components of the J-integral, namely, J_I, J_{II} and J_{III}, are calculated from J_{x_1} and J_{x_2} of Equation (15) and J_{III} of Equation (16). Since J_{III} is directly calculated, the other two are calculated by solving the equations

$$J_{x_1} = J_I + J_{II} + J_{III}$$

$$J_{x_2} = -2\sqrt{J_I J_{II}} \tag{28}$$

Equation (28) was used to obtain J_I and J_{II} as

$$J_I = \frac{1}{4}\left[\sqrt{J_{x_1} - J_{x_2} - J_{III}} + \sqrt{J_{x_1} + J_{x_2} - J_{III}}\right]^2$$

$$J_{II} = \frac{1}{4}\left[\sqrt{J_{x_1} - J_{x_2} - J_{III}} - \sqrt{J_{x_1} + J_{x_2} - J_{III}}\right]^2. \tag{29}$$

Thus, in a general mixed-mode crack problem, computation of J_{x_1} and J_{x_2} from Equation (13), J_{III} from Equation (14), and the use of Equation (29) completely defines all three modes of the J-integral. This procedure appears simple but the evaluation of J_{x_2} could be complicated and erroneous due to the numerical integration of singular functions. Furthermore, as explained in reference 23, the local crack-face displacements are needed to distinguish between the opening and sliding (shearing) modes of deformation. Because of these reasons, separation of modes using Equation (29) may not be the best choice. Hence, an alternate method that avoids the evaluation of J_{x_2}, called the decomposition method, is used.

Decomposition method.- The advantage of transforming the surface integral into a domain integral appears to be lost because of the non-zero crack-face integrals as shown in Equations (15), (16) and (27). These crack-face integrals are necessary to account for the terms containing the product of the singular and non-singular stress (strain) fields in the stress-work density expression. It was shown in reference 23 that the product terms are eliminated by decomposing the stress and displacement fields into symmetric and antisymmetric parts. The resulting equation contains only the domain integrals. Hence, the method is attractive and is computationally efficient. The decomposition method, however, requires additional effort to create a symmetric mesh about the crack plane.

The decomposition of displacement and stress fields is straight forward for 2-D problems [19, 23, 26-28], but is slightly more complicated for 3-D problems [20]. Hence, the decomposition of displacement and stress fields corresponding to the three modes of fracture is presented. Consider any two points $P(x_1, x_2, x_3)$ and $P'(x_1, -x_2, x_3)$ that are in the immediate neighborhood of the crack front and are symmetric about the crack plane as shown in Figure 2. For any arbitrarily general deformation, the displacements and stresses at points P and P' can be expressed as a combination of symmetric and antisymmetric components as shown below.

$$\begin{Bmatrix} u_{1P} \\ u_{2P} \\ u_{3P} \end{Bmatrix} = \begin{Bmatrix} u_{1S} \\ u_{2S} \\ u_{3S} \end{Bmatrix} + \begin{Bmatrix} u_{1AS} \\ u_{2AS} \\ u_{3AS} \end{Bmatrix} \tag{30}$$

and

$$\begin{Bmatrix} u_{1P'} \\ u_{2P'} \\ u_{3P'} \end{Bmatrix} = \begin{Bmatrix} u_{1S} \\ -u_{2S} \\ u_{3S} \end{Bmatrix} + \begin{Bmatrix} -u_{1AS} \\ u_{2AS} \\ -u_{3AS} \end{Bmatrix} \tag{31}$$

where subscripts S and AS denote the symmetric and antisymmetric components, respectively.

Equations (30) and (31) are used to determine the symmetric and antisymmetric displacements in terms of the displacements at points P and P' as

$$\begin{aligned} \begin{Bmatrix} u_1 \\ u_2 \\ u_3 \end{Bmatrix}_S &= \frac{1}{2} \begin{Bmatrix} u_{1P} + u_{1P'} \\ u_{2P} - u_{2P'} \\ u_{3P} + u_{3P'} \end{Bmatrix} \\ \begin{Bmatrix} u_1 \\ u_2 \\ u_3 \end{Bmatrix}_{AS} &= \frac{1}{2} \begin{Bmatrix} u_{1P} - u_{1P'} \\ u_{2P} + u_{2P'} \\ u_{3P} - u_{3P'} \end{Bmatrix} \end{aligned} \tag{32}$$

Similarly, the symmetric and antisymmetric components of the stresses are expressed in terms of the stresses at points P and P' (see Fig. 3) as

$$\begin{Bmatrix} \sigma_{11} \\ \sigma_{22} \\ \sigma_{33} \\ \sigma_{12} \\ \sigma_{23} \\ \sigma_{31} \end{Bmatrix}_S = \frac{1}{2} \begin{Bmatrix} \sigma_{11_P} + \sigma_{11_{P'}} \\ \sigma_{22_P} + \sigma_{22_{P'}} \\ \sigma_{33_P} + \sigma_{33_{P'}} \\ \sigma_{12_P} - \sigma_{12_{P'}} \\ \sigma_{23_P} - \sigma_{23_{P'}} \\ \sigma_{31_P} + \sigma_{31_{P'}} \end{Bmatrix}$$

$$\begin{Bmatrix} \sigma_{11} \\ \sigma_{22} \\ \sigma_{33} \\ \sigma_{12} \\ \sigma_{23} \\ \sigma_{31} \end{Bmatrix}_{AS} = \frac{1}{2} \begin{Bmatrix} \sigma_{11_P} - \sigma_{11_{P'}} \\ \sigma_{22_P} - \sigma_{22_{P'}} \\ \sigma_{33_P} - \sigma_{33_{P'}} \\ \sigma_{12_P} + \sigma_{12_{P'}} \\ \sigma_{23_P} + \sigma_{23_{P'}} \\ \sigma_{31_P} - \sigma_{31_{P'}} \end{Bmatrix} \tag{33}$$

The symmetric and antisymmetric displacement and stress fields are further separated into mode I, mode II, and mode III components as follows

$$\{u\} = \{u\}^I + \{u\}^{II} + \{u\}^{III}$$

$$\begin{aligned} &= \frac{1}{2} \begin{Bmatrix} u_{1P} + u_{1P'} \\ u_{2P} - u_{2P'} \\ u_{3P} + u_{3P'} \end{Bmatrix} \\ &+ \frac{1}{2} \begin{Bmatrix} u_{1P} - u_{1P'} \\ u_{2P} + u_{2P'} \\ 0 \end{Bmatrix} \\ &+ \frac{1}{2} \begin{Bmatrix} 0 \\ 0 \\ u_{3P} - u_{3P'} \end{Bmatrix} \end{aligned} \tag{34}$$

and

$$
\begin{aligned}
\{\sigma\} &= \{\sigma\}^{I} + \{\sigma\}^{II} + \{\sigma\}^{III} \\
&= \frac{1}{2}\begin{Bmatrix} \sigma_{11_P} + \sigma_{11_{P'}} \\ \sigma_{22_P} + \sigma_{22_{P'}} \\ \sigma_{33_P} + \sigma_{33_{P'}} \\ \sigma_{12_P} - \sigma_{12_{P'}} \\ \sigma_{23_P} - \sigma_{23_{P'}} \\ \sigma_{31_P} + \sigma_{31_{P'}} \end{Bmatrix} \\
&+ \frac{1}{2}\begin{Bmatrix} \sigma_{11_P} - \sigma_{11_{P'}} \\ \sigma_{22_P} - \sigma_{22_{P'}} \\ 0 \\ \sigma_{12_P} + \sigma_{12_{P'}} \\ 0 \\ 0 \end{Bmatrix} \\
&+ \frac{1}{2}\begin{Bmatrix} 0 \\ 0 \\ \sigma_{33_P} - \sigma_{33_{P'}} \\ 0 \\ \sigma_{23_P} + \sigma_{23_{P'}} \\ \sigma_{31_P} - \sigma_{31_{P'}} \end{Bmatrix}
\end{aligned} \tag{35}
$$

Similar equations in reference 20 had typographical errors. The mode I, mode II, and mode III displacements (Eq. (34)) and stresses (Eq. (35)) are used to directly evaluate J_I, J_{II}, and J_{III} from J_{x_1} using Equation (15). Note that the surface integral in Equation (15) is required only when the crack face is loaded. The J_{x_2} integral for each of these modes of deformation is identically equal to zero because of the orthogonality of the modes of deformations. Hence, the decomposition method involves only the evaluation of domain integrals and is computationally efficient.

S-Functions

As mentioned previously, the S-function is an arbitrary but continuous function with a zero value on the surface A and at the ends of the tube (A_1 and A_2) and a non-zero value (varying between zero and one) on the surface A_ϵ (see Fig. 1). On the tube surface A_ϵ, the S-function is a function of only x_3 and has a value

of one at the location where the J-integral is required. The S-functions are conveniently defined by specifying the values of S at the nodes and using the element shape functions (see Appendix). Figure 4 presents several types of S-functions for domains spanning one or two elements in the x_3-direction. Table 1 presents the values of f (see Eq. (12)) that correspond to each of the S-functions shown in Figure 4. Also, the S-functions for both 8-noded and 20-noded isoparametric elements are presented. For the 8-noded element, a linear S-function is defined, while for 20-noded elements several combinations of linear and quadratic functions are defined. Note that the values for f depend only on the variation of the S-function in the x_3-direction.

The J-integrals for various cracked 3-D solids were calculated using the various S-functions presented in Figure 4. The results of these numerical experiments will be discussed later.

RESULTS AND DISCUSSION

The EDI method was applied to several pure mode-I, mode-II, mode-III, and mixed-mode fracture problems to evaluate the accuracy, domain independency, and S-function independency. Although the method formulated above is for general anisotropic and nonlinear materials, the results presented here are restricted to linear elastic and isotropic materials with Poisson's ratio of 0.3. Throughout the analysis only *non-singular* elements were used around the crack front. Wherever possible, a *rectangular* arrangement of finite elements was used near and around the crack front to evaluate the accuracy of the rectangular type of modeling.

First, the EDI method was applied to a 3-D cracked body subjected to a combination of known mode-I, mode-II, and mode-III singular stress fields. Then, the method was applied to various finite size crack problems subjected to loadings that produce single or mixed-mode deformations. The specimen configurations considered were the middle-crack tension specimen and embedded cracks in circular cylindrical rods subjected to tension, torsion, and shearing loads. The computed J-integral values are compared with those from literature wherever possible. Both the direct and decomposition methods were used to separate the mode-III component. Only the decomposition method was used to separate mode-I and mode-II components because of the singular integration involved in the direct

method [23]. All of the above analyses used finite element models with 20-node isoparametric elements. Typical results are also presented for models with 8-node isoparametric elements.

Singular Field Loading on a Cracked Body

Consider a single-edge cracked specimen with a straight crack front as shown in the Figure 5(a). This crack configuration was subjected to mode-I, mode-II or mode-III or a combination of these modes. This problem demonstrated the accuracy of the method without introducing the nonsingular stress field that occurs in any finite-element analysis of a cracked body. The displacements in each of the three modes of deformation are given in terms of the spherical coordinates $(r, \theta,$ and $z)$ [29] as

Mode-I displacements:

$$\begin{aligned} u_1 &= \frac{K_I}{G}\sqrt{\frac{r}{2\pi}}\cos\frac{\theta}{2}\left[1 - 2\nu + \sin^2\frac{\theta}{2}\right] \\ u_2 &= \frac{K_I}{G}\sqrt{\frac{r}{2\pi}}\sin\frac{\theta}{2}\left[2 - 2\nu - \cos^2\frac{\theta}{2}\right] \\ u_3 &= 0 \end{aligned} \tag{36}$$

Mode-II displacements:

$$\begin{aligned} u_1 &= \frac{K_{II}}{G}\sqrt{\frac{r}{2\pi}}\sin\frac{\theta}{2}\left[2 - 2\nu + \cos^2\frac{\theta}{2}\right] \\ u_2 &= \frac{K_{II}}{G}\sqrt{\frac{r}{2\pi}}\cos\frac{\theta}{2}\left[-1 + 2\nu - \sin^2\frac{\theta}{2}\right] \\ u_3 &= 0 \end{aligned} \tag{37}$$

Mode-III displacements:

$$
\begin{aligned}
u_1 &= 0 \\
u_2 &= 0 \\
u_3 &= \frac{K_{III}}{G}\sqrt{\frac{2r}{\pi}}\,\sin\frac{\theta}{2}
\end{aligned}
\tag{38}
$$

where $G = E/(2(1+\nu))$

The above displacement fields were imposed on the cracked body shown in Figure 5(a). The resulting stresses and displacements in the solid were used to calculate the J-integrals by the EDI method.

Utilizing the symmetries in the problem, a representative quarter of the solid was modeled with 20-node isoparametric elements as shown in Figure 5(b). One layer of elements was used to model the entire thickness. The finite element model had 320 nodes and 36 elements. The displacements for each mode of deformations were calculated at each node of the model from Equations (36)-(38) and were used as input for EDI algorithm.

Domains and S-functions.- Five domains were used in the calculations. These domains are shown in Figure 5(b) as D_1, $D_2, \ldots D_5$. Each domain consisted of one *ring* of four elements around the crack front. The surface that is nearest to the crack front of each domain corresponds to the surface A_ϵ. Similarly, the surface that is farthest from the crack front of each domain corresponds to the surface A. (Thus, for example, the surface A for the domain D_2 will be the surface A_ϵ for domain D_3.) On the surfaces A of each domain, the S-function was prescribed to be zero. On the surfaces A_ϵ several types of S-functions in the x_3- direction (the six types are shown in Fig. 4) were considered. Since one layer of elements was used to model the thickness of the solid, Δ_2 was set equal to zero for the Type II through VI S-functions.

J-integral results.- Table 2 presents the normalized value of J_{x_1} calculated for four domains (D_2 to D_5) and six types of S-functions. The imposed displacement field on the model corresponds to $K_I = 1$. The J_{II} integral, as expected, was computed to the order of machine zero and hence is not shown here. Results for all four domains and Type I, II, III, and V S-functions are in excellent

agreement with the exact solution. Type IV and VI S-functions are quadratic in radial direction. Although these results are within two percent of the exact solution they are not as accurate as other types. Similar trends were observed when quadratic S-functions were used on several other crack problems. These results suggest that the simple Type-I S-function will give accurate J-integrals.

The computed integrals were inaccurate when the domain D_1 was used. The J_{x_1}-integrals for this domain were about 10 to 15 percent higher than those for other domains. This behavior is attributed to the errors in the numerical integration of the imposed singular stress field.

Note that in the above analysis one ring of elements around the crack front was used in each domain. Multiple rings of elements in each domain (for example, combining the D_2 and D_3 domains) gave results identical to those with a single ring of elements. Multiple rings, however, increase the data preparation efforts considerably. Thus, domains with a minimum number of rings of elements (in this case one ring) are preferable.

The domain independency observed in this example is expected since this is a plane-strain problem where the strength of the singularity is constant along the crack front (x_3-axis). Therefore, for crack bodies having a constant singularity strength along the crack front, the J_{x_1}-integral is independent of the domain.

Table 3 presents the normalized J_{x_1}, calculated assuming several linear combinations of the K_I, K_{II}, and K_{III} displacement fields given by Equations (36-38). Four domains, each with Type I S-functions were used. The J_{x_1} calculated for four domains from Equation (15) agrees very well with the exact solutions. The maximum difference is less than 2% for the $K_I = K_{II} = 1$ loading in domain D_3.

Middle-Crack Tension Specimen

A typical middle-crack tension, $M(T)$*, specimen of $W/a = 2$, $t/a = 1$, $H/a = 8$, and crack length a subjected to a uniform tension stress σ at $x_2 = \pm H/2$ was analyzed. The F-E mesh shown in the Figure 6 was used for the analysis by imposing symmetry conditions at $x_1 = -a$, $x_2 = 0$ (on the uncracked plane), and $x_3 = 0$ planes. The model was comprised of six unequal layers with thicknesses 0.22t, 0.13t, 0.08t, 0.04t, 0.02t, and 0.01t as shown in Figure 6(a). (The layer with

* ASTM abbreviation for middle-crack tension

the smallest thickness is near the $x_3 = t/2$ surface.) Five domains, D_1, D_2,... D_5, as shown in Figure 6(b) and Type I S-function (linear in radial direction and quadratic in x_3-direction, see Table 1) were used to calculate the domain integrals.

Plane-strain analysis.- First, the $M(T)$ specimen was analyzed for a plane-strain condition by imposing $u_3 = 0$ on $x_3 = 0$ and $x_3 = t/2$ planes. The J_{x_1} values were calculated for the five domains all along the crack front using each of the six layers in the thickness direction. The average normalized value of J_{x_1}, $J_{x_1} E/[\pi \sigma^2 a(1 - \nu^2)]$, was 1.410 with a maximum variation of less than 0.1%. This value agrees very well with handbook value of 1.414 and VCCT method [6] value of 1.424. These results also suggest that a simple linear S-function in the radial direction yields accurate J_{x_1} values.

Three-dimensional analysis.- The $M(T)$ specimen was reanalyzed by relaxing the plane-strain condition, i.e., by removing the boundary condition $u_3 = 0$ on the $x_3 = t/2$ plane. Three domain definitions, D_A, D_B, and D_C, were used. The domain and S-function definitions for domain D_3 are illustrated in the Figure 6(b). In D_A, each ring of elements around the crack front represents a domain. In this case, the radius (ϵ) of the inner surface (the A_ϵ surface on which the J_{x_1} is evaluated) was different for each domain; it varied from 0.0 to 0.734 times the crack length a for domains D_1 to D_5, respectively. The other two domains (D_B and D_C) involve a constant inner surface A_ϵ and a variable outer surface. Domain D_B had $\epsilon = a/10$, and, hence, the domain D_3 included the second and third rings of elements around the crack front. The corresponding S-function definition in the radial direction is bilinear as shown in the Figure 6(b). The domain D_C had $\epsilon = 0$. Therefore, for example, domain D_3 included first, second, and third rings of elements.

Table 4 presents the normalized J_{x_1} for all five domains using the three domain definitions. As expected, J_{x_1} for the interior layer is independent of the domain and the domain definition. In contrast, J_{x_1} for the last layer with a D_A domain definition shows a strong domain dependency. As the radius (or mean distance from the crack front) of the inner surface of the domain becomes large the stress, strain, and displacement fields on this surface also include the effect of the singular field from the other segments of the crack front. Evaluation of J_{x_1}-integral on this

surface would yield values which are different if the single crack front segment alone had contributed to the deformation field. If the inner surface of the domain is close to or at the crack front, the interaction from the neighboring segments of the crack is either very small or nonexistent. Hence, the D_B ($\epsilon/a = .1$) and D_C domain definitions gave more accurate results than the type D_A. These results suggest that the radius of the inner surface should be less than or equal to one-tenth of the crack front. Furthermore, a domain consisting of only one ring of elements is sufficient to calculate accurate values of J provided the domain is very close to the crack front. Note that domains D_1 and D_2 always satisfy the above conditions, hence, the results were accurate and agreed very well with the VCCT method [6].

The global average value of J_{x_1} over the crack front, however, is domain independent. Any ring of elements (even with a D_A domain definition) spanning the complete length of the crack front yields accurate values. For example, the global average value of J_{x_1}, $E\,J_{x_1}/[\pi\,\sigma^2\,a\,(1-\nu^2)]$, for the four domains were 1.521 (D_2), 1.523 (D_3), 1.529 (D_4), and 1.531 (D_5). Only the innermost domain was less accurate, 1.433 (D_1), because of errors in the stress-strain fields very near the crack front. In the above analyses a D_A domain definition was used and each ring had 24 elements.

Figure 7 compares the normalized J_{x_1} along the crack front from EDI and VCCT [6] methods. Excellent agreement is observed between the two methods. Plane-strain results are also shown in the figure as a reference solution.

Embedded Penny Shaped Crack in Circular Rod

An embedded penny shaped crack of radius a in a circular cylindrical rod with $D/a = 10$ and $H/a = 40$ is shown in Figure 8. Two types of loadings, uniform tension and torsion, were considered. Note that $\bar{x}_1$, $\bar{x}_2$, and $\bar{x}_3$ represent the global coordinate system and $\bar{u}_1$, $\bar{u}_2$, and $\bar{u}_3$ represent the corresponding displacements. Utilizing the symmetry in the problem one-eighth of the specimen was modeled. Figure 8(b) shows the F-E model of the lower eighth of the specimen. The model has 5143 nodes and 1020 twenty-noded elements with 6 layers in the circumferential direction as shown in Figure 8(b). Figure 8(c) shows the details of the modeling near a point on the crack front and the two domains D_1 and D_2 used in EDI

calculations. Note the rectangular arrangement of elements. This arrangement is in contrast to the polar arrangement used in previous examples and by other investigators [20]. Two domains and Type I S-functions were used to evaluate the integrals.

Remote tension load.- The solid is loaded by a uniform stress σ on the $\bar{x}_3 = \pm H/2$ planes. The J_{x_1}-integrals were calculated for the two domains (D_A domain definition) in each of the six layers in the circumferential direction. The J_{x1} values for all six layers calculated in either D_1 or D_2 were identical. This is expected because of the axisymmetric nature of the problem. The normalized $E\,J_{x_1}/[\sigma^2\,a(1-\nu^2)]$ values from the EDI method for domains D_1 and D_2 are 1.333 and 1.299, respectively. The exact analytical solution due to Sneddon [30] for a penny shaped crack in an infinite solid is 1.273, while Benthem and Koiter's asymptotic solution [31] for a finite size solid is 1.275. Thus, the normalized J_{x1} values from domains D_1 and D_2 differed by less than 3% from each other and are about 2% to 5% higher than the closed form solutions [30, 31]. The result for domain D_2 is more accurate than that for domain D_1, about 2% higher than Benthem and Koiter's value. The larger error in the domain D_1 may be attributed to the fact that only two elements were used around the crack front and the whole domain is within the singular field. A D_C domain definition of domain D_2, which included the two rings of elements around the crack, also gave results identical to the D_2 domain solution.

Remote torsion loading.- A torque of magnitude $T = \pi\,a^4 G/H$ was imposed at the two ends of the specimen ($\bar{x}_3 = \pm H/2$), where $G = E/[2(1+\nu)]$. This corresponds to an angular twist of magnitude $2/H$ in the uncracked rod. The displacement field for this loading in the uncracked rod is

$$\begin{aligned} \bar{u}_1 &= -(2/H)\,\bar{x}_3\,\bar{x}_2 \\ \bar{u}_2 &= (2/H)\,\bar{x}_3\,\bar{x}_1 \\ \bar{u}_3 &= 0 \end{aligned} \tag{39}$$

The boundary conditions $\bar{u}_1 = 0$ on $\bar{x}_2 = 0$ plane, $\bar{u}_2 = 0$ on $\bar{x}_1 = 0$ plane, and $\bar{u}_3 = 0$ at all nodes were imposed on the finite-element model. On the face

$\bar{x}_3 = -H/2$ the displacements given by Equation (39) were imposed on the model. The $J-$integral was calculated using both the direct and decomposition methods. The normalized values, $E\,J_{III}\,a^5\,/[(1+\nu)\,T^2]$, from the direct method for domains, D_1 and D_2 are 0.2402 and 0.2389, and from the decomposition method for domains D_1 and D_2 are 0.2388 and 0.2374, respectively. The value of the normalized integral for an infinite solid obtained with the analytical solution by Lowengrub and Sneddon [32] was 0.2293. Since only mode-III loading was applied the total integral J_{x_1} (Equation (15)) and the J_{III} integral (Equation (16)) are nearly identical for both domains. The value of J_{III} calculated by the EDI method is about 4% larger than Lowengrub and Sneddon's infinite body solution [32].

Inclined Embedded Penny Shaped Crack

The EDI algorithm is next applied to problems involving mixed-mode deformations. Figure 9 shows an embedded inclined penny shaped crack in a circular rod subjected to a uniform stress σ. The crack plane is inclined at an angle α to the $\bar{x}_1 - \bar{x}_2$ plane. The solution to this problem can be obtained as the sum of two solutions: the solution to a penny shaped crack subjected to traction normal to the crack faces of the magnitude $\sigma_n = (\sigma/2)(1 + \cos 2\alpha)$ and the solution of a penny shaped crack subjected to shear traction on the crack faces of magnitude $\tau = -(\sigma/2)\sin 2\alpha$. The exact solutions for an infinite solid with the above mentioned traction are given by Cherepanov [12] for $\nu = 0$ and Kassir and Sih [33] for a general value of Poisson's ratio ν. The strain energy release rates for the three modes, after converting the stress-intensity factors given in reference 33 using plane-strain assumptions, are

$$
\begin{aligned}
G_I &= \frac{\sigma^2\,a}{\pi\,E}(1 + \cos 2\alpha)^2 \\
G_{II} &= \frac{4(1-\nu^2)\,a\,\sigma^2}{\pi\,(2-\nu)^2\,E}\sin^2 2\alpha\,\cos^2\phi \\
G_{III} &= \frac{4(1-\nu)(1-\nu^2)\,a\,\sigma^2}{\pi\,(2-\nu)^2\,E}\sin^2 2\alpha\,\sin^2\phi
\end{aligned}
\tag{40}
$$

Where ϕ is the angle measured from the $\bar{x}_1'$-axis on the crack plane (see Fig. 9(b)). These results for the infinite size solid are used to compare with the results from EDI method for a finite size rod.

A cylindrical rod with a $D/a = 5$ and $H/a = 10$ was used in the analysis. Utilizing the symmetry in the problem one-half of solid was modeled. The model has 9547 nodes and 2000 twenty-noded parabolic elements (see Fig. 10). Symmetry conditions ($\bar{u_2} = 0$) were imposed on $\bar{x_2} = 0$ plane. The three domains D_1, D_2, and D_3 used are shown in Figure 10(b). The normalized total J-integral all along the crack front calculated using Equation (15) (J_{x1}) and the total value of J (sum of J_I, J_{II}, and J_{III}) from the decomposition method are shown in Figure 11. The Kassir and Sih [33] solution is shown by the solid line in the figure. The total values of J from the direct and the decomposition methods agree with each other for all three domains. EDI results from all three domains are about 2% to 7% larger than Kassir and Sih's solution because a finite size solid was analyzed. Among the three domains, the domain D_2 gave the lowest value while the domain D_3 gave the largest. The maximum difference between the two domains D_2 and D_3 was about 3 percent.

Figure 12(a) shows the distribution of the normalized J_I, J_{II}, and J_{III} values along the crack front obtained from the decomposition method. The individual mode components from the EDI method agree well with those determined by Kassir and Sih all along the crack front. The small differences between the two solutions can be attributed to the finite solid. It is interesting to note that Cherepanov's solutions (with $\nu = 0$) for J_{II} and J_{III} are about 28% lower than Kassir and Sih solution (with $\nu = 0.3$).

Figure 12(b) compares the J_{III} values calculated from the direct (Equation (16)) and decomposition methods with Kassir and Sih solution [33]. For all three domains, the two EDI procedures agree well with each other and with Kassir and Sih.

Inclined Semi-Circular Surface Crack in a Tension Rod

A semi-circular prismatic rod with an inclined semi-circular surface crack was analyzed. The centrally located semi-circular surface crack plane is oriented at an angle 30^0 to the $\bar{x}_1$-axis of the rod (see the insert sketch in Fig. 13). The rod is subjected to a remote tension loading. The finite-element model of Figure 10(a) was utilized to analyze this problem. The three domains D_1, D_2, and D_3 shown in Figure 10(b) were used in the EDI calculation. The total value

of $J(J_{x_1})$ and the individual components J_I, J_{II}, and J_{III} along the crack front are shown in Figures 13 and 14, respectively. These results were obtained using the decomposition method. No reference solutions are available for this problem. Solid lines in Figures 13 and 14 are the smooth fit to the domain D_2 solutions.

The J-values for the three domains agree well with one another. The maximum difference between the results of the domain D_2 and D_3 is about 3 percent. As expected, (a) all the J values are symmetric about $\phi = 90^0$, (b) the J_I and J_{II} have the highest values at $\phi = 0^0$ and 180^0 with the lowest value at $\phi = 90^0$, (c) the J_{III} value is zero at $\phi = 0^0$ and 180^0, (d) J_{III} value is maximum at $\phi = 90^0$ and (e) J_{II} value is zero at $\phi = 90^0$.

Application to 8-Node Isoparametric Elements

The use of 8-noded isoparametric elements in the EDI analysis was demonstrated using two classical crack problems in a tension specimen: an embedded elliptic crack and a penny shaped surface crack. The F-E model and the domain used were same as that given in reference 34, except the notch radius is zero. The F-E mesh had 3420 nodes and 2772 eight- noded elements. Around the crack front, a rectangular arrangement of non-singular elements was used (similar to that shown in Fig. 8(c)). The element size around the crack front was a/20, where a is the crack length in thickness direction of specimen. A domain consisting of the second ring of elements around the crack front and two element layers along the crack front was used for the J-integral calculation.

Figure 15 compares the distribution of the normalized total $J(J_{x_1})$ along the crack front for an embedded elliptic crack calculated from the EDI method to Green and Sneddon's infinite body solution [35]. The two solutions agree well with each other.

Figure 16 shows the distribution of the normalized total J (which is same as J_I) along the crack front for a semi-circular surface crack in a tension specimen. The J-values from the EDI method agree very well with those from the VCCT [6] and Raju and Newman's solutions [36]. The EDI algorithm is incorporated in the ZIP3D [37] code. The ZIP3D is an elastic and elastic-plastic finite-element code to analyze cracked bodies.

CONCLUDING REMARKS

Details of development of the three dimensional equivalent domain integral (3-D EDI) method for the calculation of mixed-mode fracture mechanics parameters in isotropic or anisotropic and linear or nonlinear materials are presented. Differences and improvements between the current algorithm and that reported in the literature are highlighted. Results presented in this paper are restricted to isotropic elastic solutions. Several single and mixed-mode loaded cracked bodies were analyzed and results were found to agree very well with those available in the literature.

The EDI method with 20- or 8-noded isoparametric, nonsingular elements and either a polar or rectilinear arrangement of elements at the crack front gives accurate values of the J-integral. A simple linear S-function in the radial direction is recommended if only one ring of elements at the crack front is used. The EDI method was found to be independent of the type of S-function, except for one special case. The J values were found to be inaccurate for domains consisting of only one ring of elements around the crack front with S-functions that were quadratic in the radial direction from the crack front.

The EDI method is domain independent provided the radius of the inner surface of the domain is either zero or very small (less than one-tenth of the major crack length). Domains consisting of only the second ring of elements or the first two rings of elements around the crack front reduce the data preparation effort and also give accurate J-integral values.

The principal advantage of the 3-D EDI method is that the finite element idealization need not be orthogonal to the crack front. The orthogonality of the modeling at the crack front is a requirement for the virtual crack closure and the force methods. In the case of mixed-mode loadings, the decomposition method yielded accurate J-integrals. The method requires the evaluation of only one integral with different sets of displacement and stress fields. However, the method requires a finite element mesh that is symmetric about the crack plane.

ACKNOWLEDGEMENTS

This work was performed under NASA contract NAS1-18599, NASA Langley Research Center, Hampton, VA 23665-5225.

REFERENCES

1. D. M. Parks, "A stiffness derivative finite element technique for determination of crack tip stress intensity factor," Int. J. Fract., Vol. 10, 1974, pp. 487-502.
2. D. M. Parks, "The virtual crack extension method for nonlinear material behavior," Comp. Meth. Appl. Mech. Engng., Vol. 12, 1977, pp. 353-364.
3. T. K. Hellen, "On the method of virtual crack extension," Int. J. Numer. Meth. in Engng., Vol. 9, 1975, pp. 187-207.
4. T. K. Hellen, "Virtual crack extension methods for non-linear materials," Int. J. Numer. Meth. Engng., Vol. 28, 1989, pp. 929-942.
5. E. F. Rybicki and M. F. Kanninen, "A finite element calculation of stress intensity factors by modified crack closure integral," Engng. Fract. Mech., Vol. 9, No. 4, 1977, pp. 931-938.
6. K. N. Shivakumar, P. W. Tan, and J. C. Newman, "Virtual crack closure technique for calculating stress-intensity factors for cracked three-dimensional bodies," Int. J. Fract., Vol. 36, 1988, pp. R43-R50.
7. I. S. Raju, K. N. Shivakumar, and J. H. Crews Jr., "Three- dimensional elastic analysis of a composite double cantilever beam specimen," AIAA J., Vol. 26, No. 12, 1988, 1493-1498.
8. F. G. Buchholz, "Improved formulae for the finite element calculation of the strain energy release rate by the modified crack closure integral method," In Accuracy Reliability and Training in FEM-Technology (Ed. J. Robinson), Robinson and Associates, Dorest, 1984, pp. 650-659. Mech., Vol. 31, 1967, pp. 503-512.
9. J. R. Rice, "A path-independent integral and the approximate analyses of strain concentration by notches and cracks," J. Appl. Mech., Vol. 35, 1968, pp. 376-386.
10. G. P. Cherepanov, "Crack propagation in continuous media," J. Appl. Math. Mech., Vol. 31, 1967, pp. 503-512.
11. J. D. Eshelby, "The continuum theory of lattice defects," in Solid State Physics (Edited by F. Seitz and D. Turnbull) Vol. III, Academic Press, New York, 1956, pp. 79-144.
12. G. P. Cherepanov, Mechanics of Brittle Fracture, Translated and Edited by R. W. De Wit and W. C. Cooly, McGraw Hill, New York, 1979.

13. F. Z. Li, C. F. Shih, and A. Needleman, "A comparison of methods for calculating energy release rates," Engng. Fract. Mech., Vol. 21, 1985, pp. 405-421.
14. K. Kishimoto, S. Aoki, and M. Sakata, "Energy-release rate in elastic plastic problems," J. Appl. Mech. Vol.48, 1981, pp. 825-829.
15. K. Kishimoto, S. Aoki, and M. Sakata, "Energy flux in to the process region in elastic-plastic fracture problems," Engng. Fract. Mech., Vol. 20, 1984, pp. 827-836.
16. S. N. Atluri, "Path independent integrals in finite elasticity and inelasticity, with body force, inertia and arbitrary crack-face conditions," Engng. Fract. Mech., Vol. 16, 1982, pp.341-364.
17. T. Nishioka and S. N. Atluri, "Path-independent integrals, energy release rate and general solutions of near-tip fields in mixed-mode dynamics fracture mechanics," Engng. Fract. Mech., Vol. 18, 1983, pp. 1-22.
18. F. W. Burst, J. J. McGowan, and S. N. Atluri, "A combined numerical study of ductile crack growth after a large unloading, using T*, J, and CTOA criteria," Engng. Fract. Mech., Vol. 23, 1986, pp. 537-550.
19. G. P. Nikishkov and S. N. Atluri, "An equivalent domain integral method for computing crack-tip integral parameters in non-elastic, thermo-mechanical fracture," Engng. Fract. Mech., Vol. 26, 1987, pp. 851-867.
20. G. P. Nikishkov and S. N. Atluri, "Calculation of fracture mechanics parameters for an arbitrary three-dimensional crack, by the 'equivalent domain integral' method ," Int. J. Numer. Meth. in Engng., Vol. 24, 1987, pp. 1801-1821.
21. N. Miyakazi, T. Watanabe, and G. Yagawa, "The virtual crack extension of J- and J^-integrals," Engng. Fract. Mech., Vol. 22, 1985, pp. 975-987.
22. B. Moran and C. F. Shih, "Crack tip and associated domain integrals from momentum and energy balance," Engng. Fract. Mech., Vol. 27, 1987, pp. 615-642.
23. I. S. Raju and K. N. Shivakumar, "Implementation of equivalent domain integral method in the two-dimensional analysis of mixed-mode problems." NASA CR-181813, April 1989.
24. H. G. de Lorenzi, "On energy release rate and the J-integral for 3-D crack configuration," Int. J. of Fract. , Vol. 19, 1982, pp. 183-192.

25. H. G. de Lorenzi, "Energy release rate calculation by finite element method," Engng. Fract. Mech., Vol. 21, 1985, pp. 129-143.
26. H. Ishikawa, "A finite element analysis of stress intensity factors for combined tensile and shear loading by only a virtual crack extension," Int. J. Fract., Vol. 16, 1980, pp. R243-R246.
27. G. T. Sha and C. T. Yang, "Weight function calculations for mixed-mode fracture problems with the virtual crack extension technique," Engng. Fract. Mech., Vol. 21, 1985, pp. 1119-11150.
28. T. Nishioka and S. N. Atluri, "On the computation of mixed-mode K-factors for a dynamically propagating crack using path-independent integrals J_K," Engng. Fract. Mech., Vol. 20, 1984, pp. 193-208.
29. P. C. Paris and G. C. Sih, "Stress analysis of cracks," Fracture Toughness Testing and Applications, ASTM STP-381, American Society for Testing and Materials, Philadelphia, PA, 1965, pp. 30-81.
30. I. N. Sneddon, "The distribution of stress in the neighborhood of an elastic solid," Proc. Roy. Soc. London, Series A 187, 1946, pp. 229-260.
31. J. P. Benthem and W. T. Koiter, "Asymptotic approximations to crack problems," Chapter 3 in "Methods of Analysis of Crack Problems", G. C. Sih, Nordhoff International Publishing, (1972).
32. M. Lowengrub and I. N. Sneddon, "The distribution of stress in the vicinity of an external crack in an infinite elastic solid," Int. J. Engng. Science, Vol. 3, 1965, pp. 451-460.
33. M. K. Kassir and G. C. Sih, "Three dimensional stress distribution around an elliptical crack under arbitrary loadings," Trans. ASME, J. Appl. Mech., Vol. 33, 1966, pp. 601-611.
34. K. N. Shivakumar and J. C. Newman, Jr., "Stress-intensity factors for large aspect ratio surface and corner cracks at a semicircular notch in tension specimen," Engng. Fract. Mech., Vol. 38, No. 6, 1991, pp. 467-473.
35. A. E. Green and I. N. Sneddon, "The distribution of stresses in the neighborhood of a flat elliptical crack in an elastic solid," Proc. Cambridge Philosophical Society, Vol. 46, 1950, p. 1950.
36. I. S. Raju and J. C. Newman Jr., "Stress-Intensity factors for a wide range of semi-elliptical surface cracks in finite-thickness plates," Engng. Fract. Mech., Vol. 11, No. 4, 1979, pp. 817-829.

37. K. N. Shivakumar and J. C. Newman, Jr., "ZIP3D - An elastic and elastic-plastic finite-element analysis program for cracked bodies," NASA TM 102753, November 1990.
38. G. C. Sih, "A review of the three-dimensional stress problem for a cracked plate," Int. J. of Fracture, Vol. 7, 1971, pp. 39-61.
39. K. N. Shivakumar and I. S. Raju, "Treatment of singularities in cracked bodies," Int. J. of Fracture, Vol. 45, 1990, pp. 159-178.

APPENDIX: NUMERICAL IMPLEMENTATION OF THE EDI METHOD

This appendix presents the numerical implementation of the EDI method for a finite element analysis with isoparametric elements. The procedure presented in this appendix is similar to that of the 2-D analysis in reference 23 and is applicable to both 8-noded and 20-noded 3-D isoparametric elements. For the purpose of illustration the 20-noded element is used.

A typical finite element model around the crack front is shown in Figure 17(a). The shaded region represents a typical domain surrounding the crack front. Although, no restriction was imposed on the number of elements in the domain either in x_1- or x_2-directions, one ring of elements in x_1- and x_2-directions were used to explain the procedure. The procedure for computing J_{x_k} is presented but can be easily extended to the J_{III} computation as well.

The total J-integral (J_{x_k}) is equivalent to sum of the domain integrals contributed by the elements in the shaded region shown in Figure 17.

$$(J_{x_k})_{domain} = \sum_{i=1}^{N_e} J_{x_{k_i}} \qquad (A1)$$

where $J_{x_{k_i}}$ is the volume integral over the i^{th} element in the shaded region and N_e is the number of elements enclosed in the domain.

For isoparametric finite elements, the displacements within the element are defined by the shape functions N_j and the nodal displacements $(u_\alpha)_j$.

$$u_\alpha = N_j(u_\alpha)_j \qquad (A2)$$

where $N_j = N_j(\xi, \eta, \zeta)$ and ξ, η, ζ are the coordinates of the parent element. The index j takes the value 1 to N_n (N_n is the number of nodes per element; $N_n = 8$ for eight-node linear element and $N_n = 20$ for twenty-node quadratic element) and α takes the value 1, 2, and 3 corresponding to the displacements in x_1-, x_2-, and x_3-directions, respectively.

The volume integral $J_{x_{k_i}}$ of the i^{th} element (Eq. (20)) is computed using Gaussian quadratures as

$$(J_{x_{k_i}})_{domain} \cdot f = - \Big[\int_{-1}^{1}\int_{-1}^{1}\int_{-1}^{1} [W\frac{\partial S}{\partial x_k} - \{u'_{x_k}\}^T [\underline{\sigma}]\{S'\}]$$

$$\times (det\ [\mathbf{J}])\ d\xi\ d\eta\ d\zeta$$

$$+ \int_{-1}^{1}\int_{-1}^{1}\int_{-1}^{1} [\frac{\partial W}{\partial x_k} - \{\sigma\}^T \{\epsilon'_{x_k}\}]\ S\ (det\ [\mathbf{J}])\ d\xi\ d\eta\ d\zeta \Big]_i$$

$$= - \Big[\sum_{m=1}^{M_G} \sum_{n=1}^{M_G} \sum_{p=1}^{M_G} \Big\{ [W\frac{\partial S}{\partial x_k} - \{u'_{x_k}\}^T[\underline{\sigma}]\{S'\}]$$

$$+ [\frac{\partial W}{\partial x_k} - \{\sigma\}^T\{\epsilon'_{x_k}\}]\ S \Big\}\ w_m w_n w_p (det[\mathbf{J}]) \Big]_i \qquad (A3)$$

where M_G is the number of Gaussian quadrature points used in each direction ξ, η, and ζ and w_m, w_n, and w_p are the Gaussian weights and det [**J**] is the determinant of the Jacobian matrix [**J**] defined by

$$[\mathbf{J}] = \begin{bmatrix} \frac{\partial N_1}{\partial \xi} & \frac{\partial N_2}{\partial \xi} \cdots & \frac{\partial N_{N_n}}{\partial \xi} \\ \frac{\partial N_1}{\partial \eta} & \frac{\partial N_2}{\partial \eta} \cdots & \frac{\partial N_{N_n}}{\partial \eta} \\ \frac{\partial N_1}{\partial \zeta} & \frac{\partial N_2}{\partial \zeta} \cdots & \frac{\partial N_{N_n}}{\partial \zeta} \end{bmatrix} \begin{bmatrix} (x_1)_1 & (x_2)_1 & (x_3)_1 \\ (x_1)_2 & (x_2)_2 & (x_3)_2 \\ \cdot & \cdot & \cdot \\ \cdot & \cdot & \cdot \\ \cdot & \cdot & \cdot \\ (x_1)_{N_n} & (x_2)_{N_n} & (x_3)_{N_n} \end{bmatrix} \qquad (A4)$$

Most of the quantities necessary for Equations (20-23), W, W^{III}, $\{\sigma\}$, $\{\sigma_3\}$, and $[\underline{\sigma}]$, are readily known in terms of the nodal displacements of the element. But, computation of the terms $S, \{S'\}$, and $\frac{\partial W}{\partial x_k}$ needs special attention and is discussed below. Evaluation of the derivative matrices $\{\epsilon'_{x_k}\}$ and $\{u'_3\}$ is same as that for $\frac{\partial W}{\partial x_k}$; hence, they are not discussed.

S-Functions

As mentioned previously, the S-function is any arbitrary but continuous function with a non-zero value (varying between 0 and 1) on the surface of the inner

tube (A_ϵ) and a value of zero on the surface of the outer tube and at the two ends of the tube (see Fig. 1). The variation of S-function over a typical i^{th} element in the shaded region is shown in the Figure 17(b). The function is conveniently defined using the element shape functions as

$$S(\xi, \eta, \zeta) = N_j S_j$$

where $j = 1$ to N_n and S_j is the nodal value of the S-function at node j on the element. Different S-functions can be defined by assigning 0, .5 or 1 to S_j. For a typical element shown in the Figure 17(b), the S-function is completely defined by specifying $S_2 = S_{10} = 1$ and zero to all other nodes. This definition yields a S-function having a parabolic variation along the crack front and a linear variation in the radial direction (Type I S-function).

Partial Derivatives of S

Once S is defined the partial derivatives of S, $\frac{\partial S}{\partial x_1}$, $\frac{\partial S}{\partial x_2}$, and $\frac{\partial S}{\partial x_3}$ can be computed using the isoparametric formulation as

$$\begin{Bmatrix} \frac{\partial S}{\partial x_1} \\ \frac{\partial S}{\partial x_2} \\ \frac{\partial S}{\partial x_3} \end{Bmatrix} = [\mathbf{J}]^{-1} \begin{Bmatrix} \frac{\partial S}{\partial \xi} \\ \frac{\partial S}{\partial \eta} \\ \frac{\partial S}{\partial \zeta} \end{Bmatrix} \qquad (A6)$$

where [J] is the Jacobian matrix defined in Equation A4.

Partial Derivatives of W

The terms $\frac{\partial W}{\partial x_k}$ are computed by fitting a bilinear equation (in terms of the parent coordinates ξ, η, and ζ) to W, using the values at the 2 x 2 x 2 integration points and then taking derivatives with respect to x_k. In reference 20, the integral $\int \frac{\partial W}{\partial x_k} dV$ was approximated by evaluating $\frac{\partial W}{\partial x_k}$ at the center of the element. A different approach is taken here. Because all the quantities are known at the integration points, the integration is carried out without further approximations of other terms in Equations (20) to (23). The values of the stresses are known to be more reliable at the 2 x 2 x 2 Gaussian points within the element (in comparison

to the nodal values). The stress-work density W is approximated in bilinear form as

$$\begin{aligned} W(\xi,\eta,\zeta) &= a_1 + a_2\xi + a_3\eta + a_4\zeta + a_5\xi\eta \\ &\quad + a_6\eta\zeta + a_7\zeta\xi + a_8\xi\eta\zeta \end{aligned} \tag{A7}$$

Using the 2 x 2 x 2 Gaussian values of the stress-work density W, Equation (A7) is rewritten as

$$W(\xi,\eta,\zeta) = [1 \quad \xi \quad \eta \quad \zeta \quad \xi\eta \quad \eta\zeta \quad \xi\zeta \quad \xi\eta\zeta\,][T]\{W_G\} \tag{A8}$$

where

$$[T] = \frac{1}{8}\begin{bmatrix} 1 & 1 & 1 & 1 & 1 & 1 & 1 & 1 \\ -\sqrt{3} & -\sqrt{3} & -\sqrt{3} & -\sqrt{3} & \sqrt{3} & \sqrt{3} & \sqrt{3} & \sqrt{3} \\ -\sqrt{3} & -\sqrt{3} & \sqrt{3} & \sqrt{3} & -\sqrt{3} & -\sqrt{3} & \sqrt{3} & \sqrt{3} \\ -\sqrt{3} & \sqrt{3} & -\sqrt{3} & \sqrt{3} & -\sqrt{3} & \sqrt{3} & -\sqrt{3} & \sqrt{3} \\ 3 & 3 & -3 & -3 & -3 & -3 & 3 & 3 \\ 3 & -3 & -3 & 3 & 3 & -3 & -3 & 3 \\ 3 & -3 & 3 & -3 & -3 & 3 & -3 & 3 \\ -3\sqrt{3} & 3\sqrt{3} & 3\sqrt{3} & -3\sqrt{3} & 3\sqrt{3} & -3\sqrt{3} & -3\sqrt{3} & 3\sqrt{3} \end{bmatrix} \tag{A9}$$

and

$$\{W_G\}^T = \{W_I \;\; W_{II} \;\; W_{III} \;\; W_{IV} \;\; W_V \;\; W_{VI} \;\; W_{VII} \;\; W_{VIII} \;\}^T \tag{A10}$$

where W_I to W_{VIII} are the values of W at the 2 x 2 x 2 Gaussian points shown in Figure 18. The partial derivatives $\frac{\partial W}{\partial \xi}$, $\frac{\partial W}{\partial \eta}$, and $\frac{\partial W}{\partial \zeta}$ are

$$\begin{Bmatrix} \frac{\partial W}{\partial \xi} \\ \frac{\partial W}{\partial \eta} \\ \frac{\partial W}{\partial \zeta} \end{Bmatrix} = \begin{bmatrix} 0 & 1 & 0 & 0 & \eta & 0 & \zeta & \eta\zeta \\ 0 & 0 & 1 & 0 & \xi & \zeta & 0 & \xi\zeta \\ 0 & 0 & 0 & 1 & 0 & \eta & \xi & \xi\eta \end{bmatrix} [T]\,[W_G] \tag{A11}$$

The derivatives $\frac{\partial W}{\partial x_k}$ can now be obtained as

$$\left\{ \begin{array}{c} \frac{\partial W}{\partial x_1} \\ \\ \frac{\partial W}{\partial x_2} \\ \\ \frac{\partial W}{\partial x_3} \end{array} \right\} = [\mathbf{J}]^{-1} \left\{ \begin{array}{c} \frac{\partial W}{\partial \xi} \\ \\ \frac{\partial W}{\partial \eta} \\ \\ \frac{\partial W}{\partial \zeta} \end{array} \right\} \qquad (A13)$$

where [**J**] is defined in Equation (A4).

Similarly, derivatives of $\{\epsilon_{x_k}\}$ and $\{u_3''\}$ can be obtained. All the necessary terms in Equations (20) to (24) are now known and, hence, the domain integrals for each element can be calculated.

Computation of J-integral Along the Crack Front

In a 3-D finite-element model of a cracked body, the crack front is divided into a number of To calculate the J-integral at each of the nodal points, for example at node i, consider the crack front segment between the nodes $(i-1)$ and $(i+1)$ (see Fig. 19). The S-function will have a value of unity at node i and zero at nodes $(i-1)$ and $(i+1)$. Since the S-function is generated from the element shape functions, the S-function is linear for 8-noded linear element and quadratic for the 20-noded quadratic element (see Fig. 19). Utilizing the domain corresponding to the crack front segment $(i-1)$ and $(i+1)$ (see, for example Fig. 17 for a 20-node model), the J-integrals are calculated from Equations (15) and (16). The analysis is repeated at other nodal locations. If the first node is on the plane of symmetry of the model, the left-half (segment $(i-1)$ to i) of the S-function is neglected. However, the accuracy of the J-integral is poor at nodes on the free surface of the model because of the well known boundary layer effect [38,39].

Table 1. S-functions and f-integrals.

S-function type	S-function		f-integral
	Left segment $\zeta = x_3/\Delta_1$	Right segment $\zeta = x_3/\Delta_2$	
I	$(1-\zeta^2)$	$(1-\zeta^2)$	$2\Delta/3$
II	$(1+\zeta)/2$	$(1-\zeta)/2$	$(\Delta_1+\Delta_2)/2$
III	$(\zeta^2-\zeta)/2$	$(\zeta^2+\zeta)/2$	$(\Delta_1+\Delta_2)/6$
IV	$(\zeta^2-\zeta)/2$	$(\zeta^2+\zeta)/2$	$(\Delta_1+\Delta_2)/6$
V	$(1+\zeta)/2$	$(1-\zeta)/2$	$(\Delta_1+\Delta_2)/2$
VI	$(1+\zeta)/2$	$(1-\zeta)/2$	$(\Delta_1+\Delta_2)/2$
8-noded element	$(1+\zeta)/2$	$(1-\zeta)/2$	$(\Delta_1+\Delta_2)/2$

Table 2. Comparision of J_{x_1} for various S-functions and domains in a $K_I = 1$ stress field loaded specimen.

S-function type	$\sqrt{J_{x_1} E/(1-\nu^2)}$			
	Domains			
	D_2	D_3	D_4	D_5
I	1.0008	1.0005	1.0013	1.0018
II	1.0008	1.0005	1.0044	1.0018
III	1.0008	1.0005	1.0107	1.0018
IV	1.0144	1.0200	1.0085	1.0062
V	1.0053	1.0070	1.0037	1.0032
VI	0.9870	0.9870	1.0129	0.9973

Table 3. Comparision of J-integral from EDI method with exact solutions for mixed-mode singular field loadings.
(Type I S-functions)

Loading			J_{x_1}				
				EDI method			
K_I	K_{II}	K_{III}	Exact	D_2	D_3	D_4	D_5
1	0	0	0.9100	0.9107	0.9105	0.9112	0.9116
0	1	0	0.9100	0.9142	0.9156	0.9127	0.9121
0	0	1	1.3000	1.3015	1.3020	1.3011	1.3010
1	1	0	1.8200	1.7929	1.7864	1.8035	1.8096
0	1	1	2.2100	2.2158	2.2176	2.2138	2.2131
1	0	1	2.2100	2.2122	2.2125	2.2123	2.2126
1	1	1	3.1200	3.0945	3.0885	3.1046	3.1106

Table 4. Comparision of normalized J calculated from various domain definitions for $M(T)$ specimen.
($W/a = 4$, $H/a = 8$, $t/a = 1$, $\nu = 0.3$)

		$E\,J_{x_1}/\{\pi\,\sigma^2 a(1-\nu^2)\}$			
		EDI method			VCCT method
z/t	Domain	Domain type			
		D_A	D_B	D_C	
0.11	D_1	1.558	1.558	1.558	1.575
(interior layer)	D_2	1.551	1.551	1.571	
	D_3	1.544	1.559	1.579	
	D_4	1.547	1.572	1.592	
	D_5	1.543	1.582	1.602	
0.495	D_1	1.293	1.293	1.293	1.279
(exterior layer)	D_2	1.380	1.380	1.296	
	D_3	1.468	1.389	1.305	
	D_4	1.498	1.400	1.316	
	D_5	1.526	1.411	1.327	

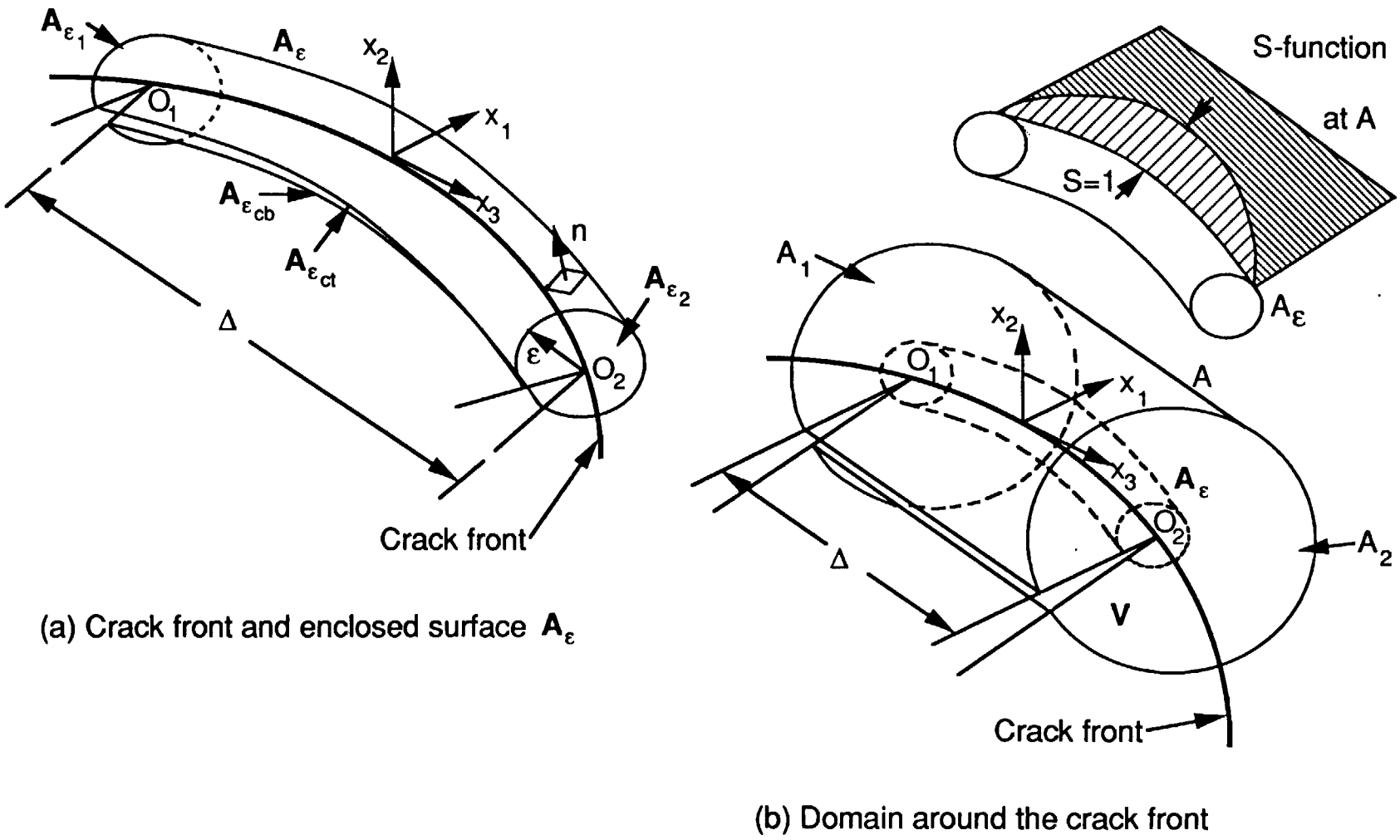

Figure 1.- Nomenclature and the domain description.

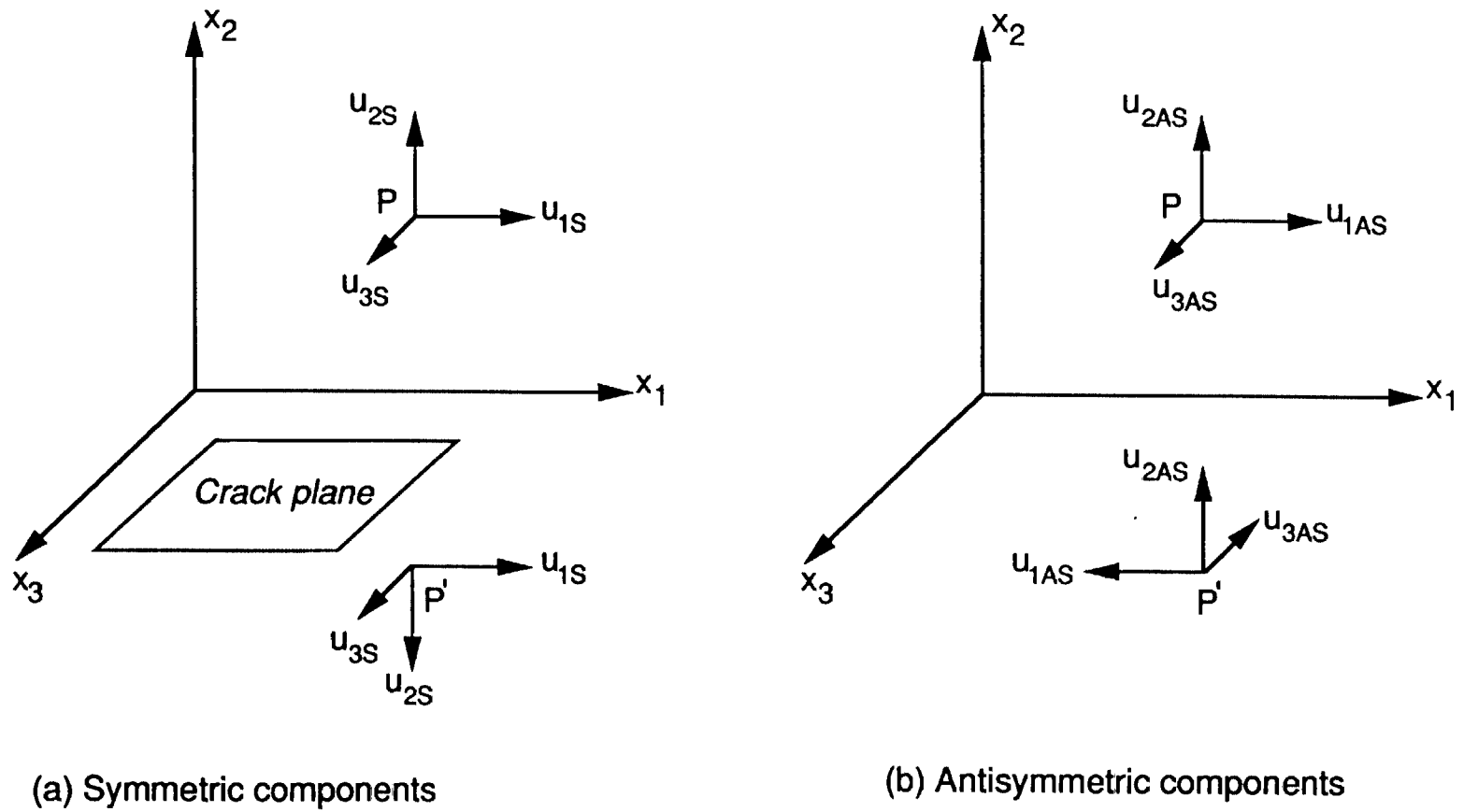

Figure 2.- Symmetric and antisymmetric displacement components.

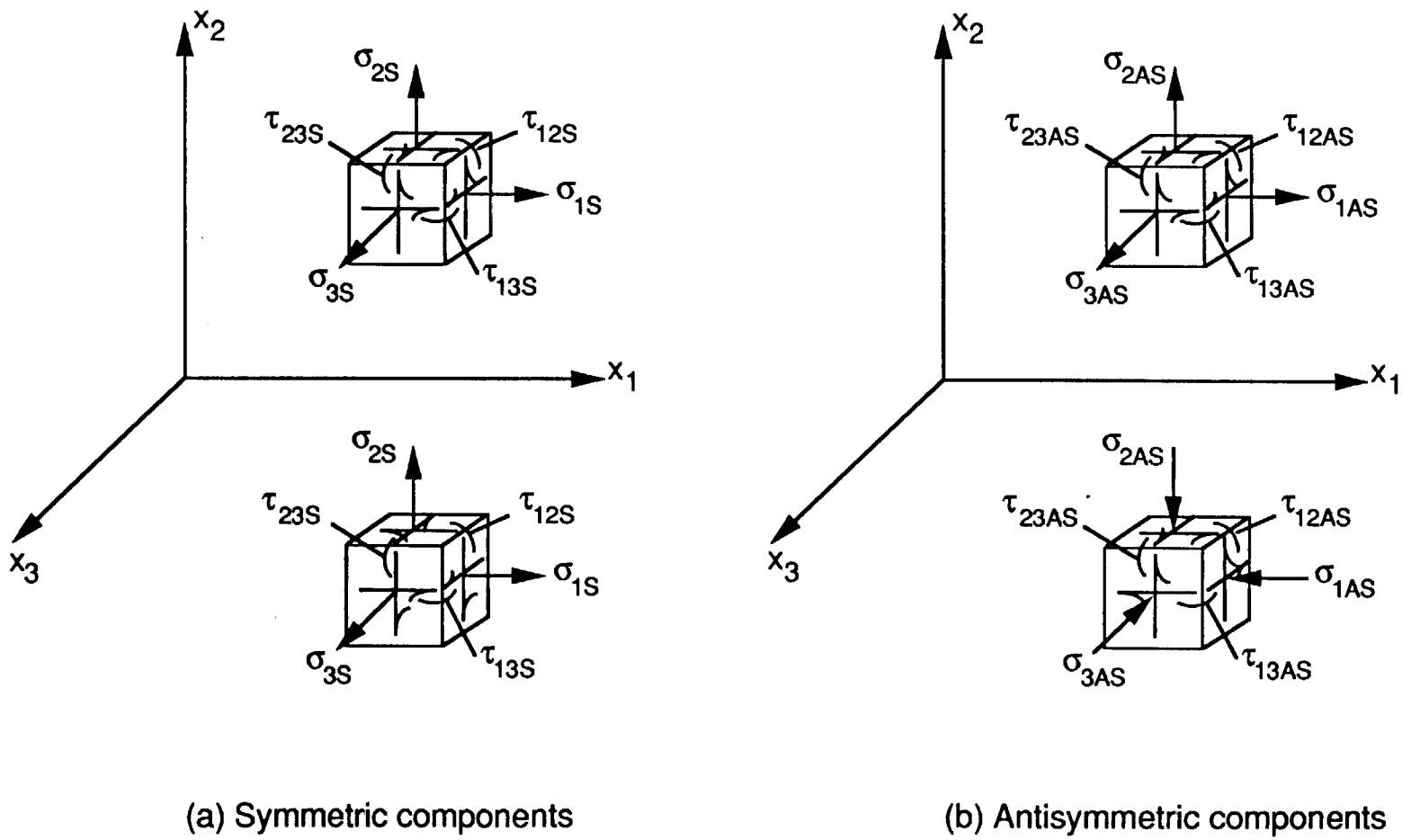

Figure 3.- Symmetric and antisymmetric stress components.

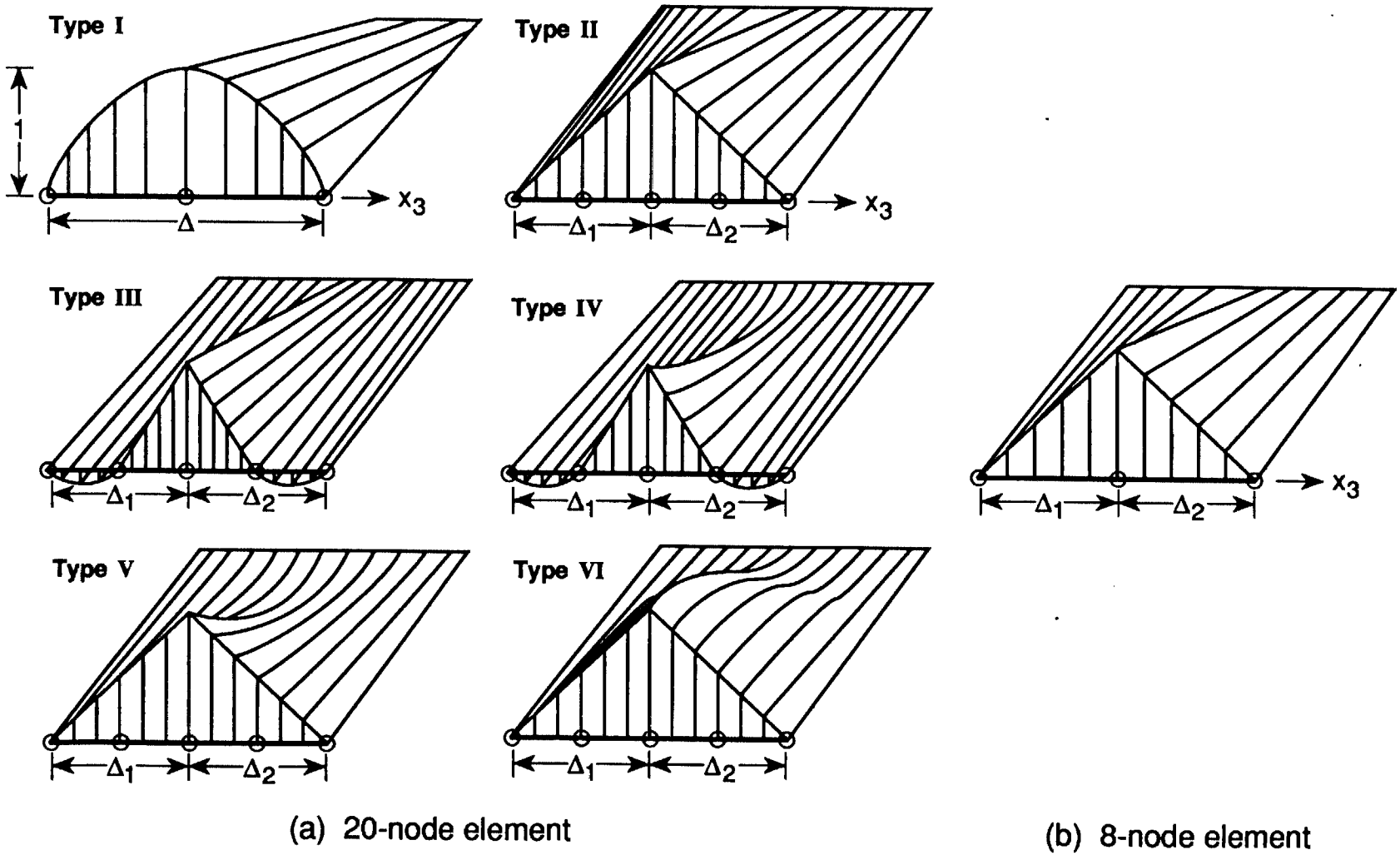

Figure 4. Definition of S-functions for 20-node and 8-node isoparametric finite-elements.

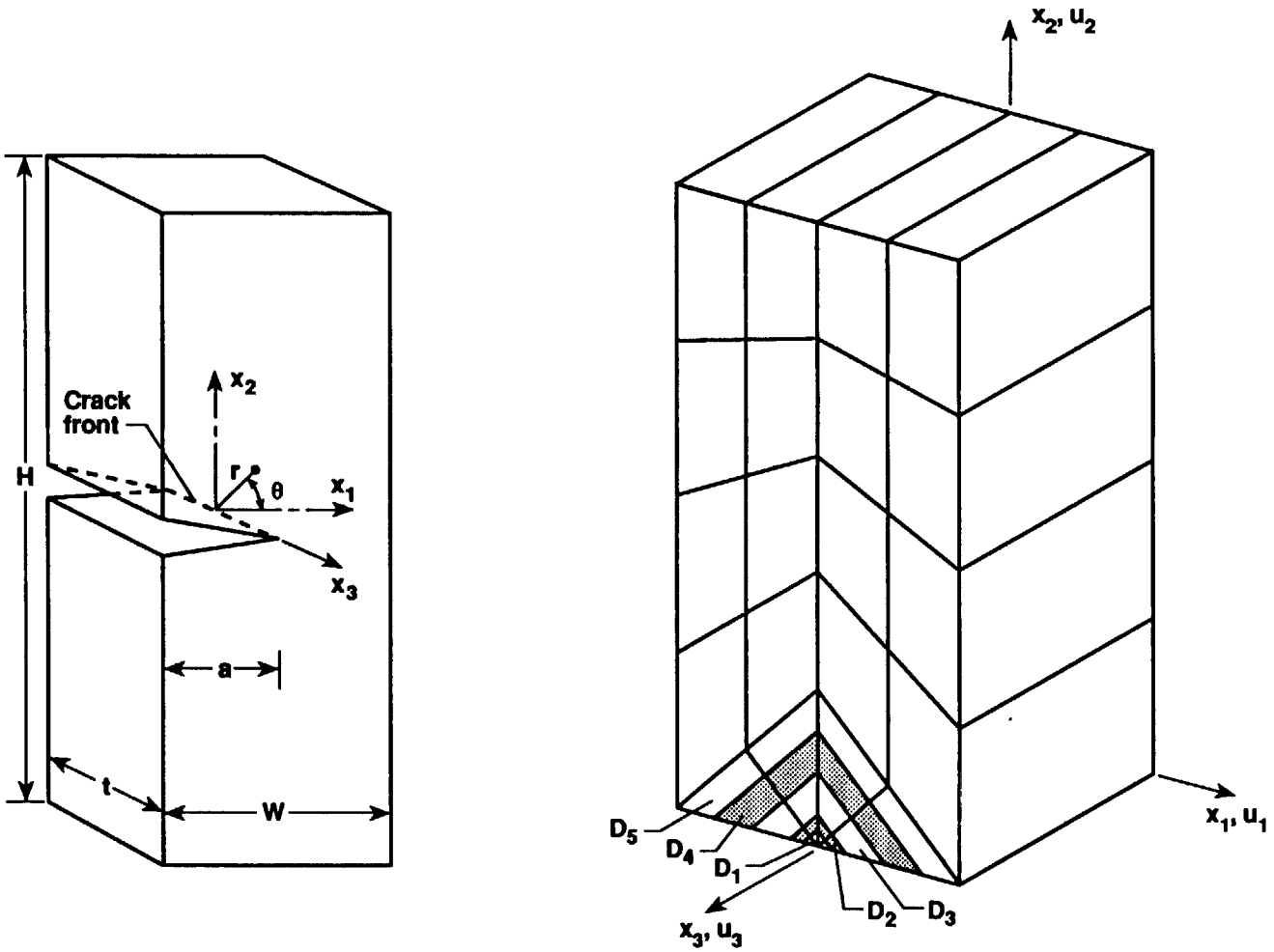

(a) Single-edge-cracked specimen

(b) Finite-element model and five domains

Figure 5. Specimen and the finite-element model.

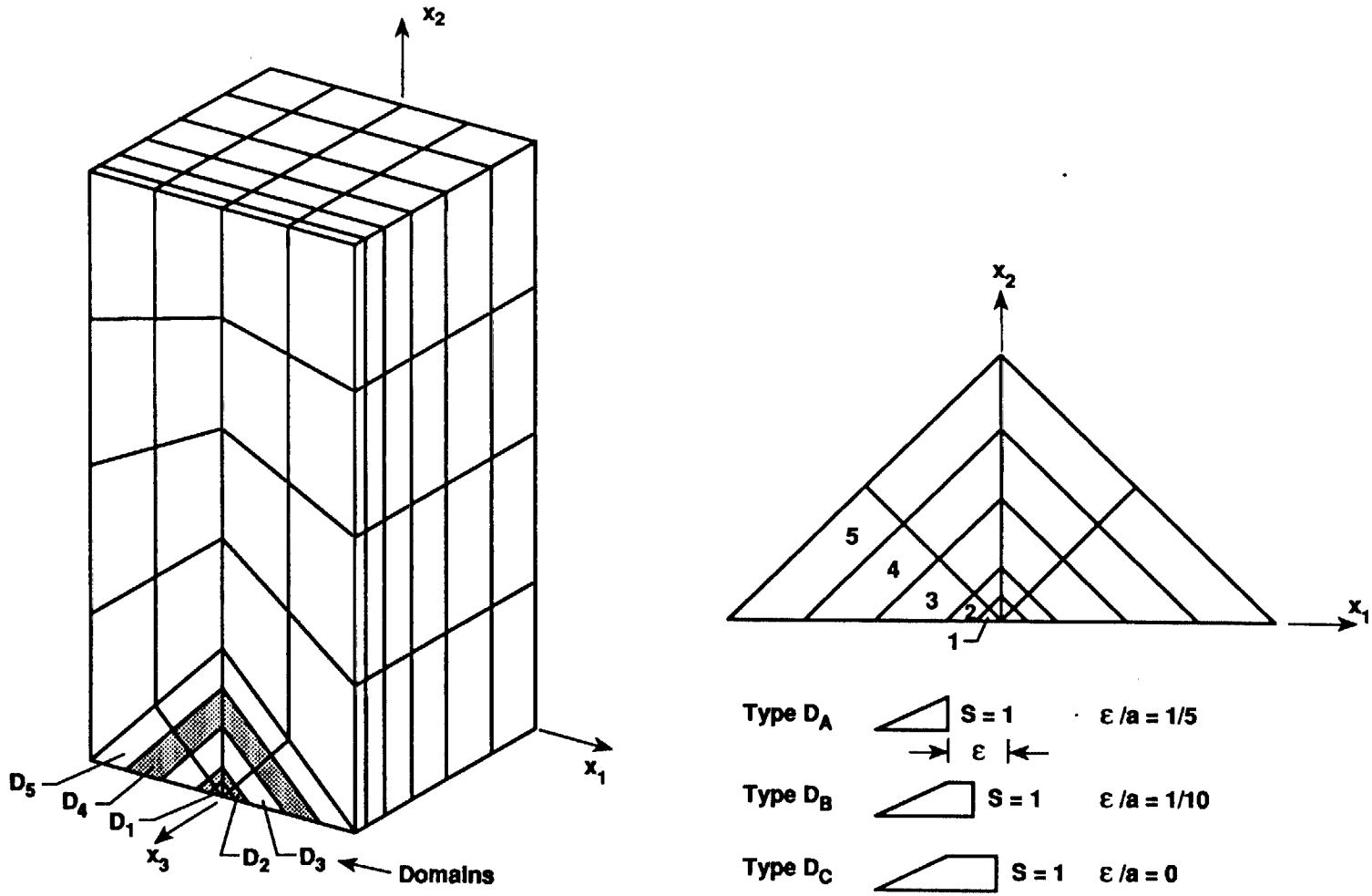

(a) Three-dimensional finite-element model

(b) Three types of domain definitions and the corresponding S-functions

Figure 6. Three-dimensional finite-element modeling of M(T) specimen.

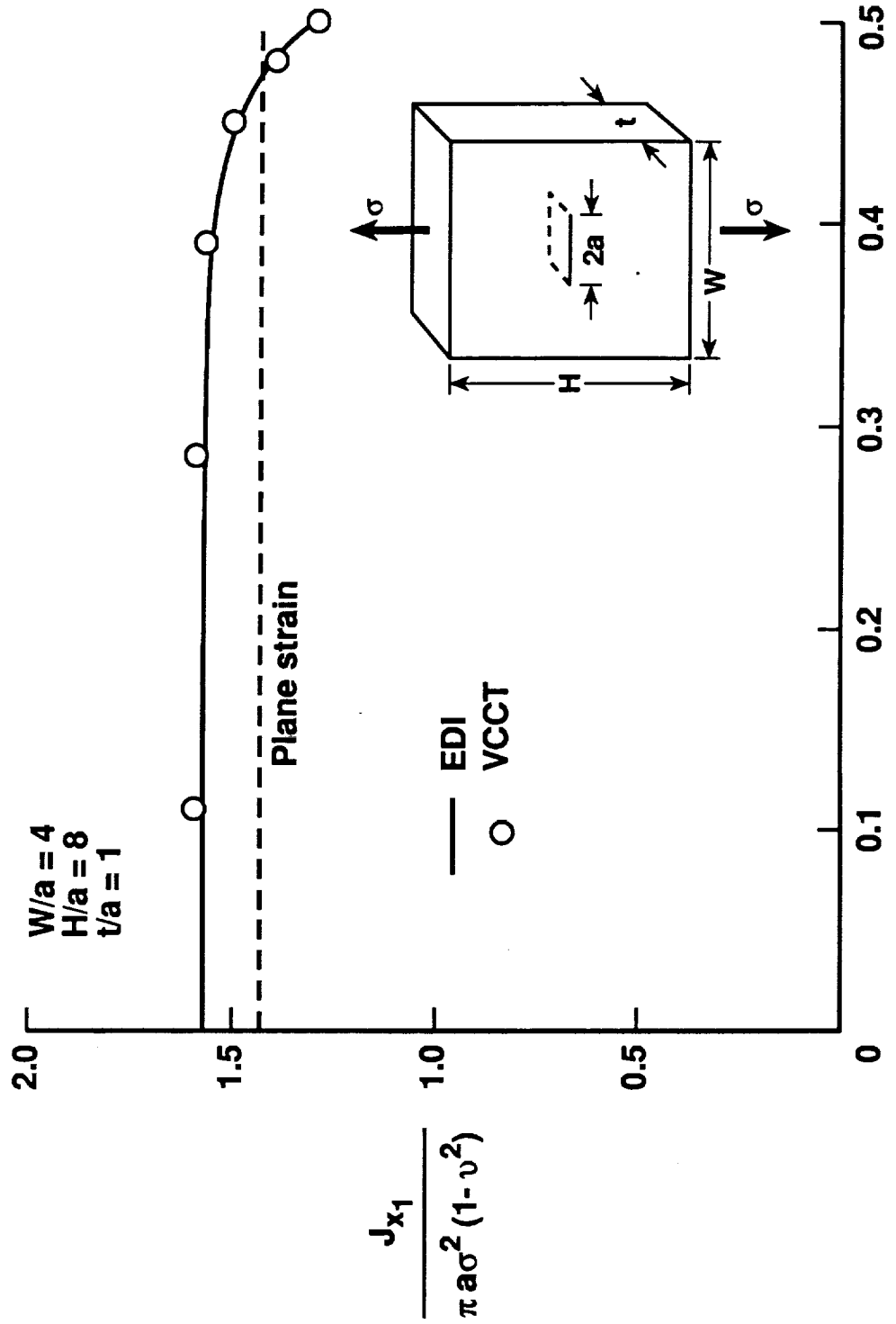

Figure 7. Variation of normalized J_{x_1} along the crack front for a M(T) specimen.

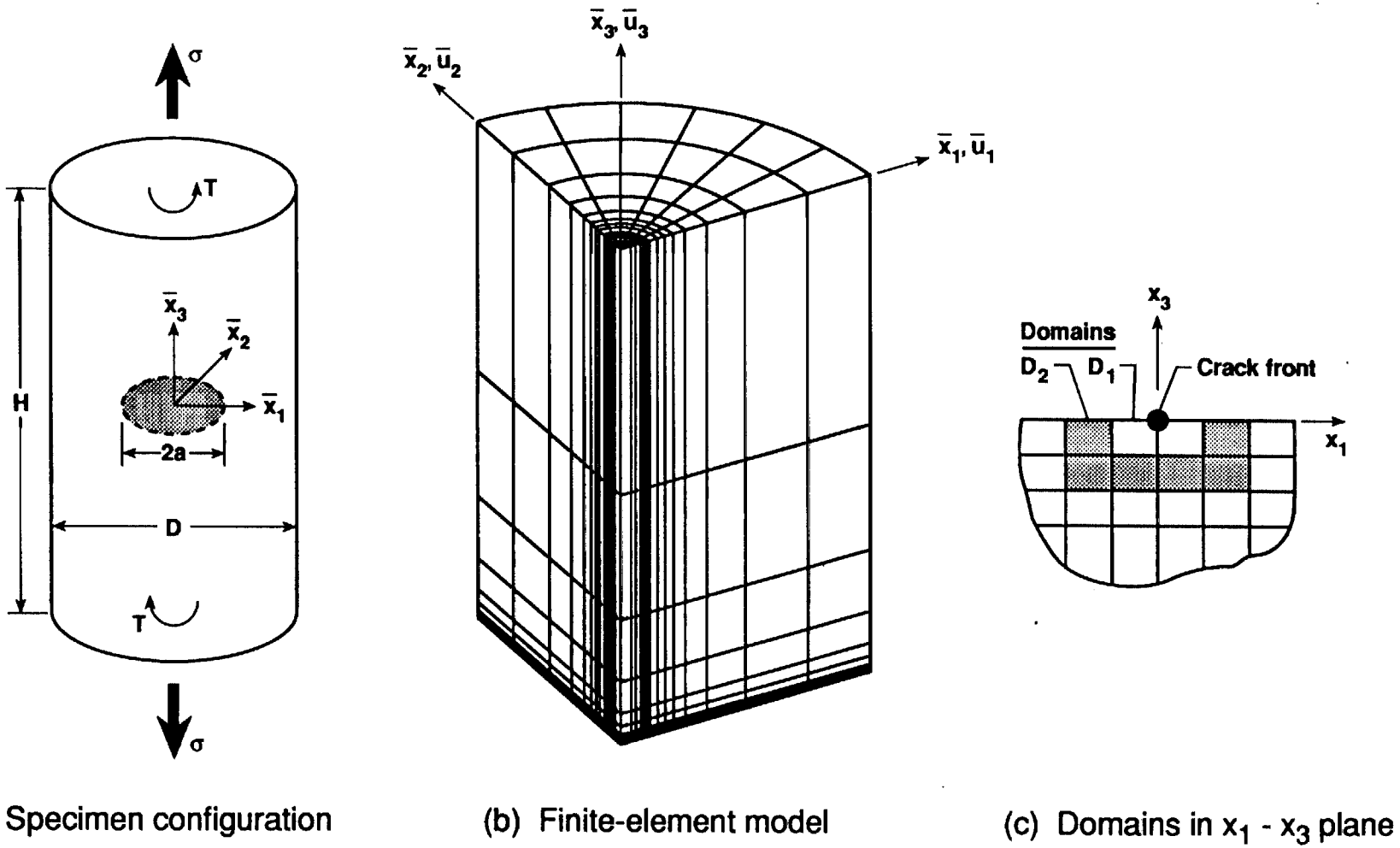

(a) Specimen configuration (b) Finite-element model (c) Domains in x_1 - x_3 plane

Figure 8. Embedded penny-shaped crack in a circular rod subjected tension and torsion loadings.

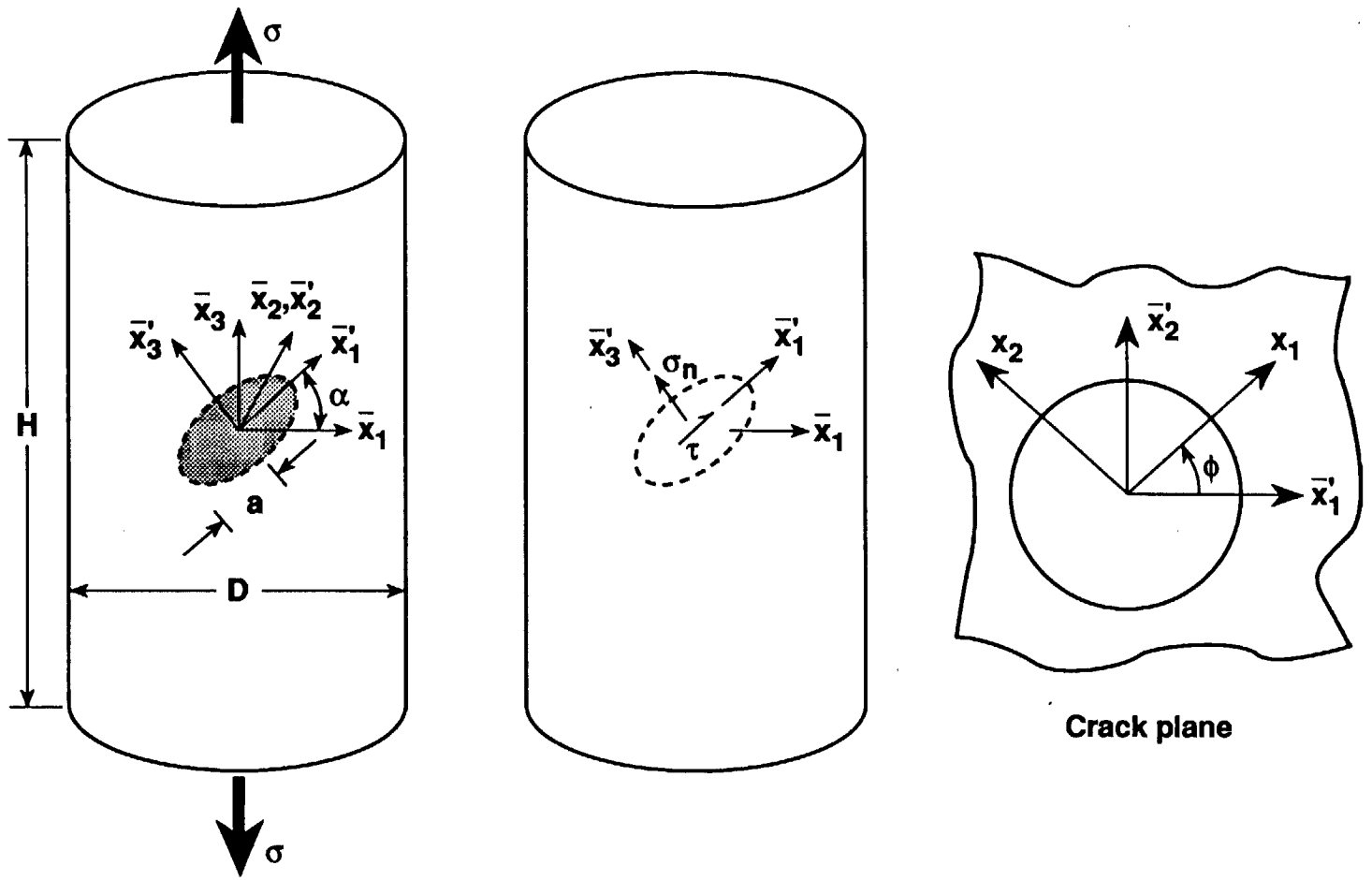

Figure 9. Inclined penny-shaped crack embedded in a circular rod under tension σ.

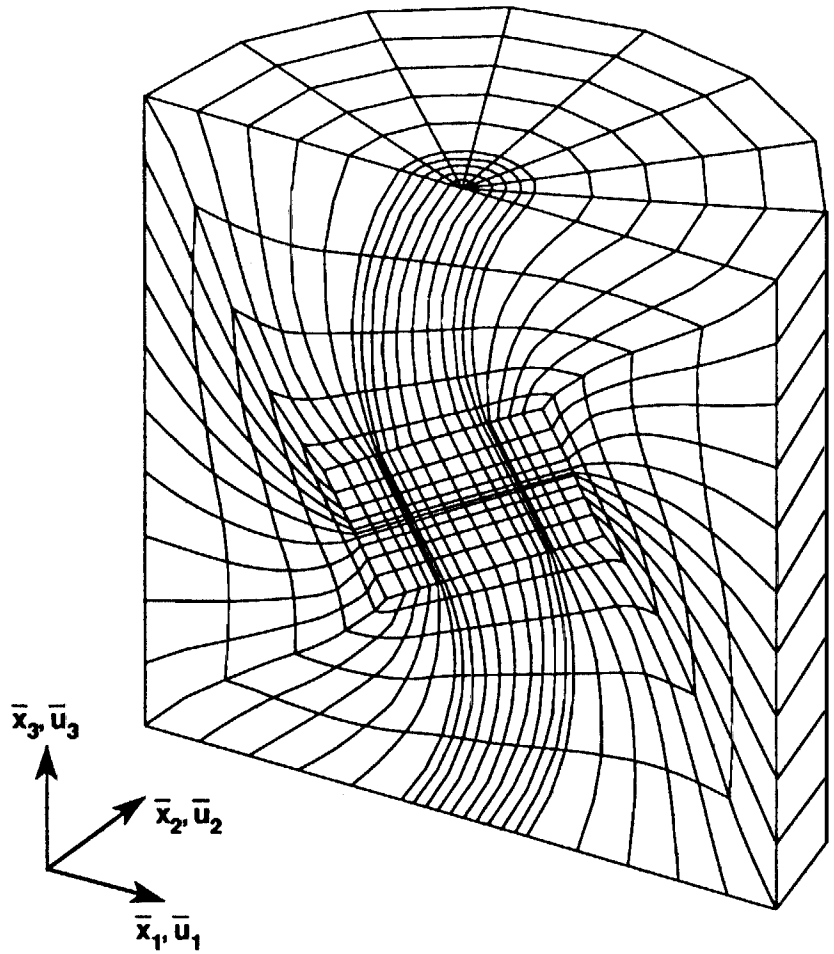

(a) Finite-element model

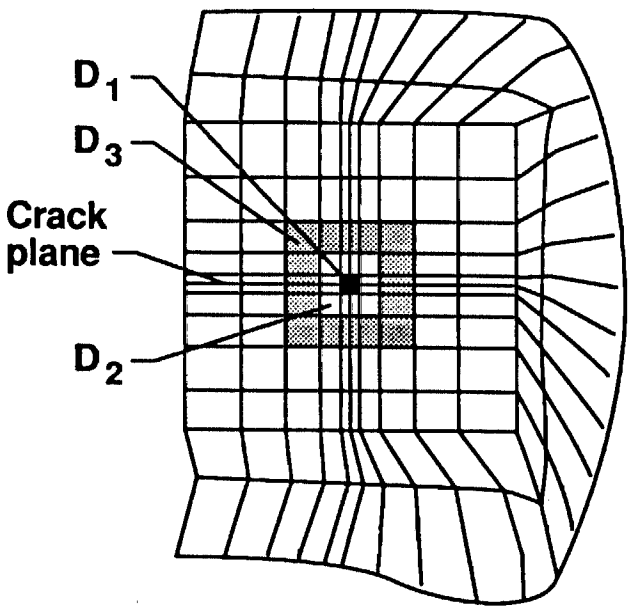

(b) Finite-element model and domains near the crack tip

Figure 10. Finite-element model for an inclined embedded penny-shaped crack.

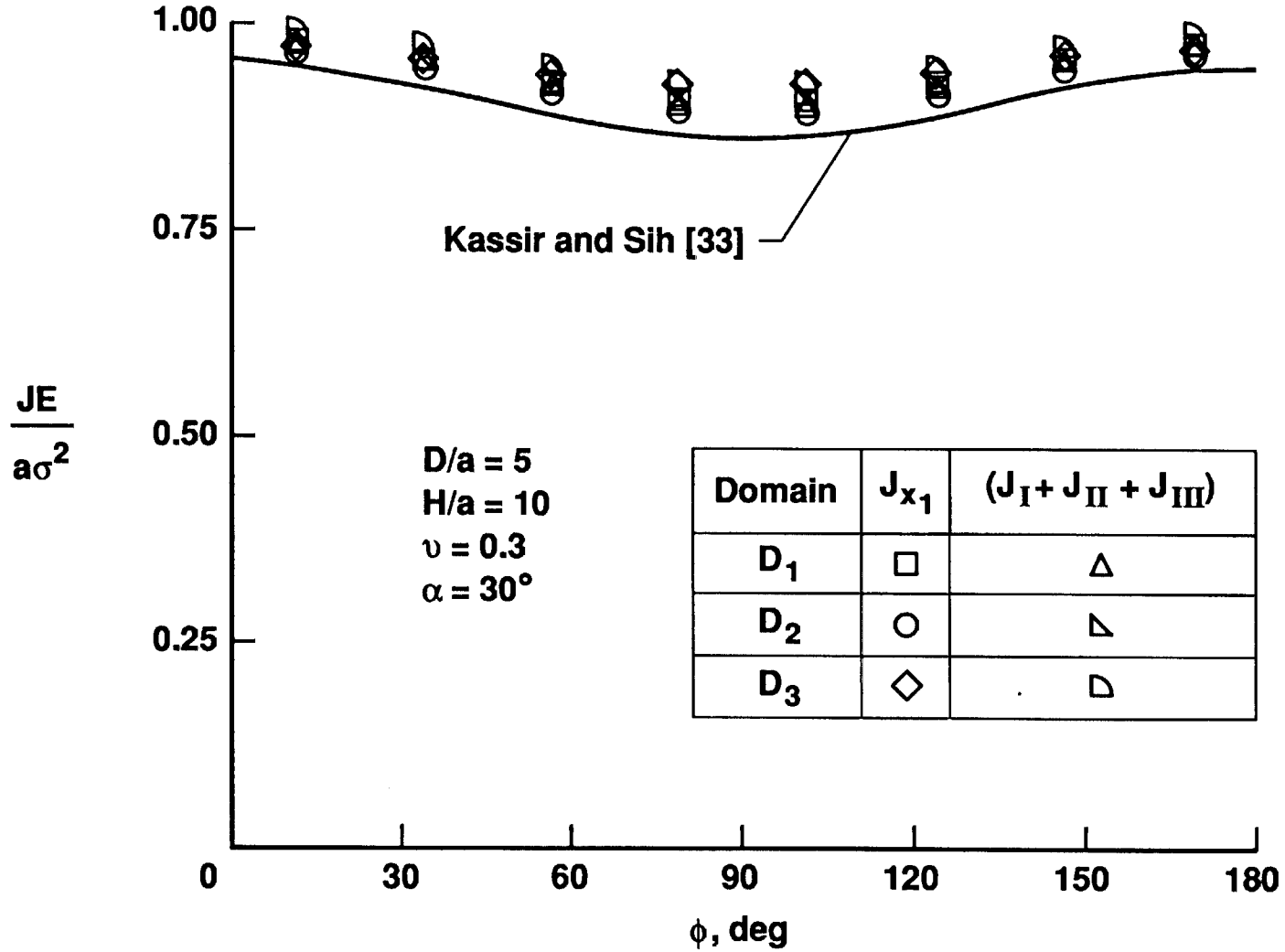

Figure 11. Normalized J-distribution along the crack front of an embedded penny-shaped crack.

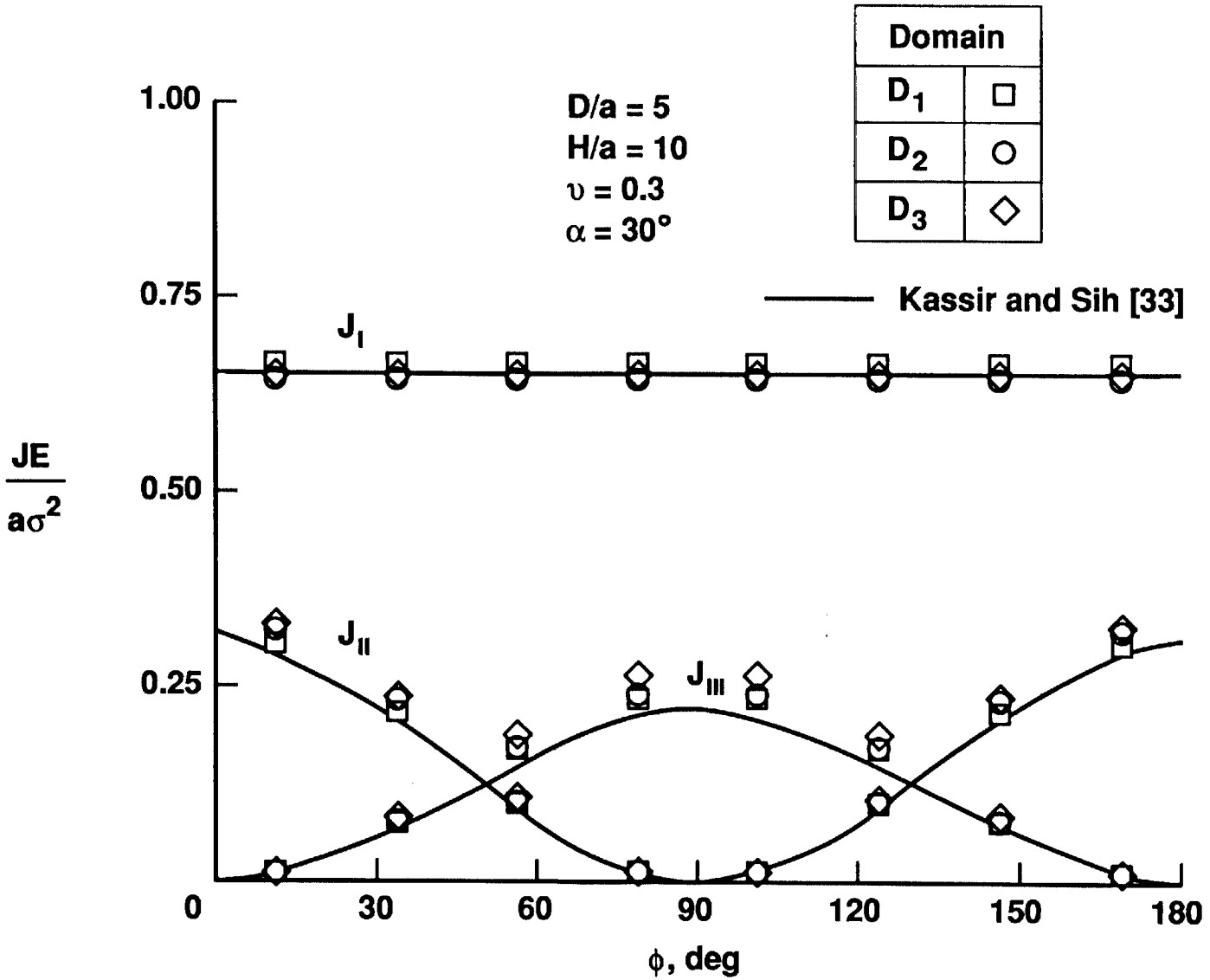

Figure 12(a). Normalized J_I, J_{II}, and J_{III} distribution along the crack front of an embedded inclined penny-shaped crack.

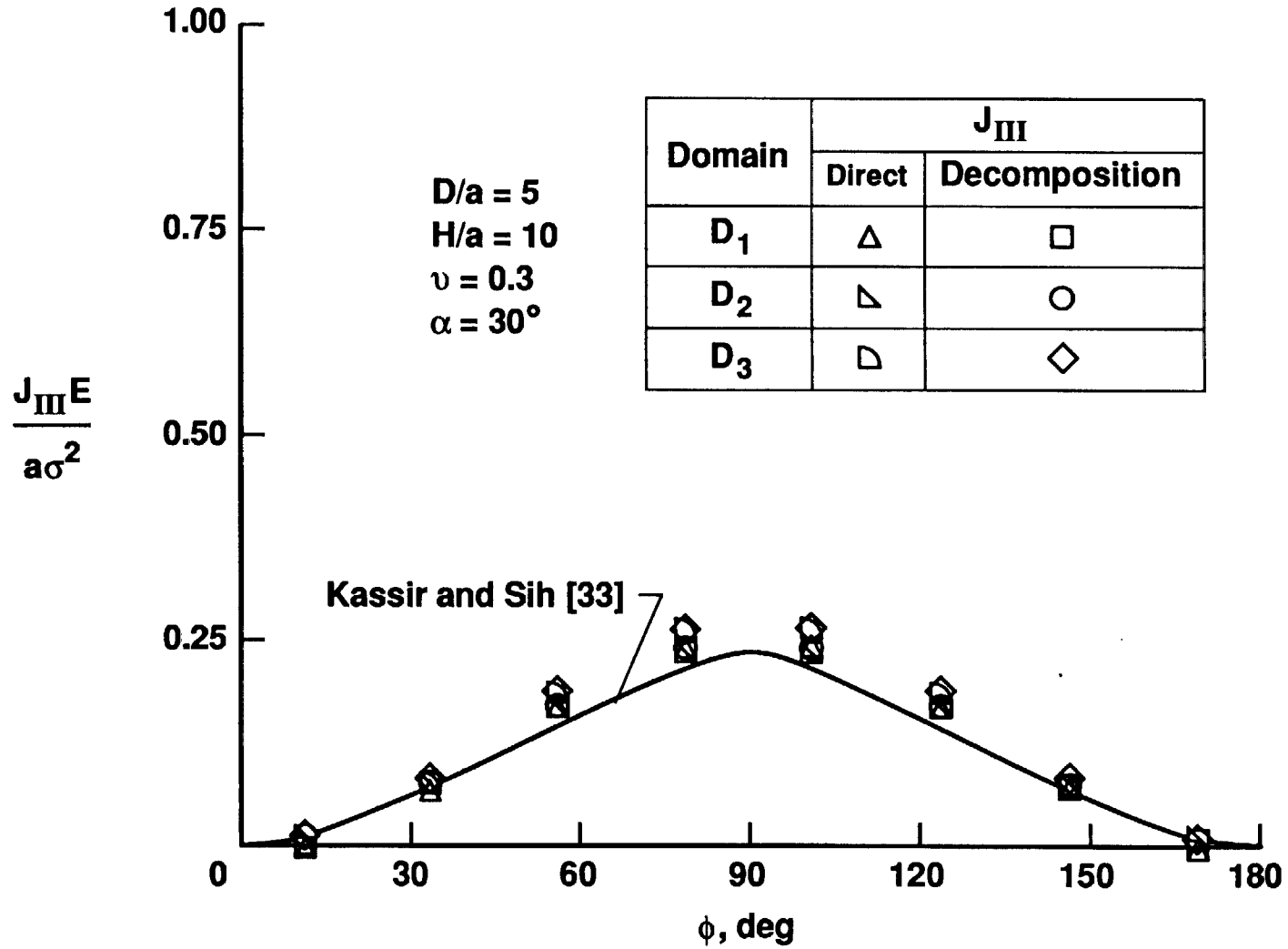

Figure 12(b). Comparison of J_{III} from direct and decomposition methods.

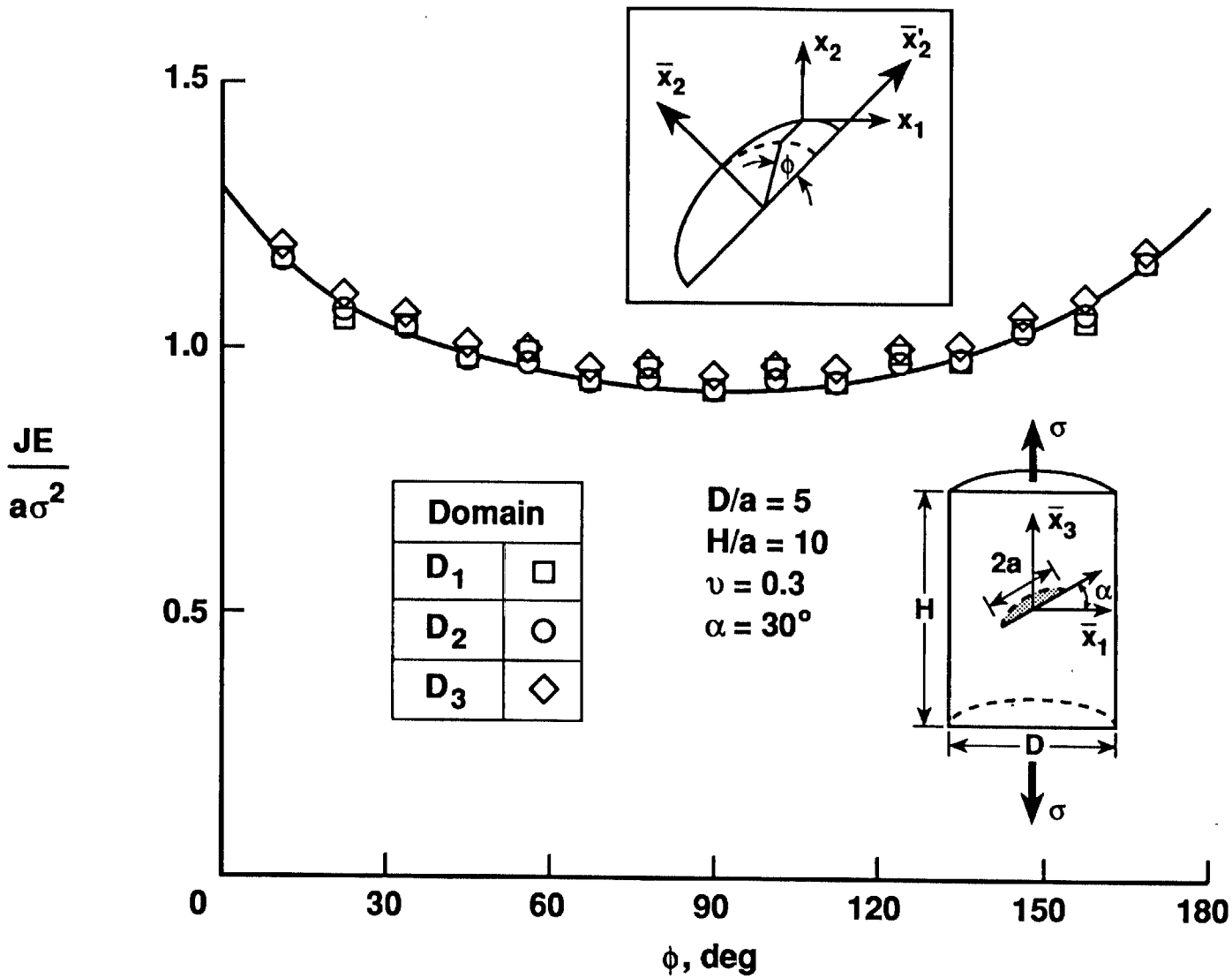

Figure 13. Normalized total J distribution along the crack front of an inclined semicircular surface crack.

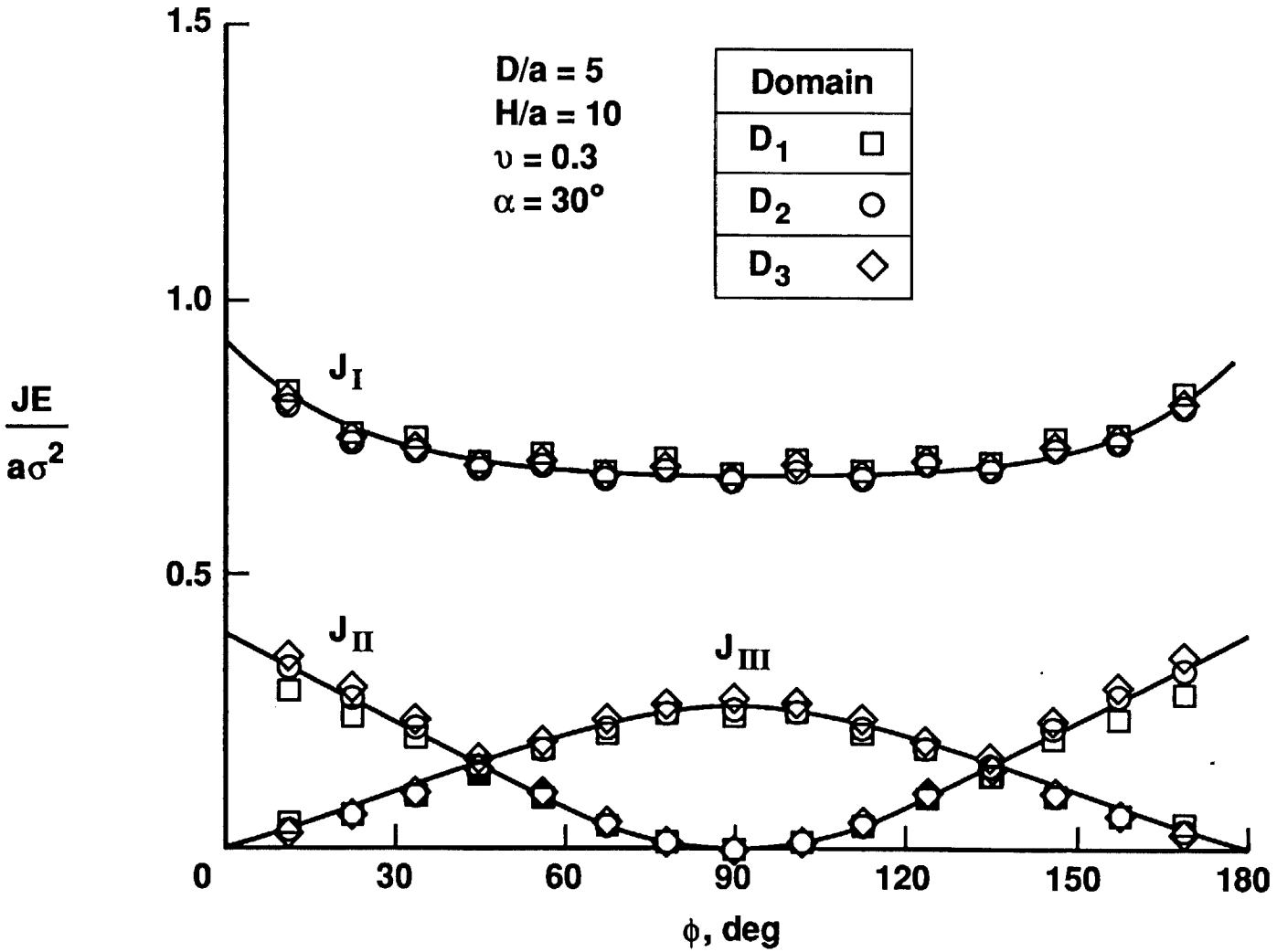

Figure 14. Normalized J_I, J_{II}, J_{III} distribution along the crack front of an inclined semicircular surface crack.

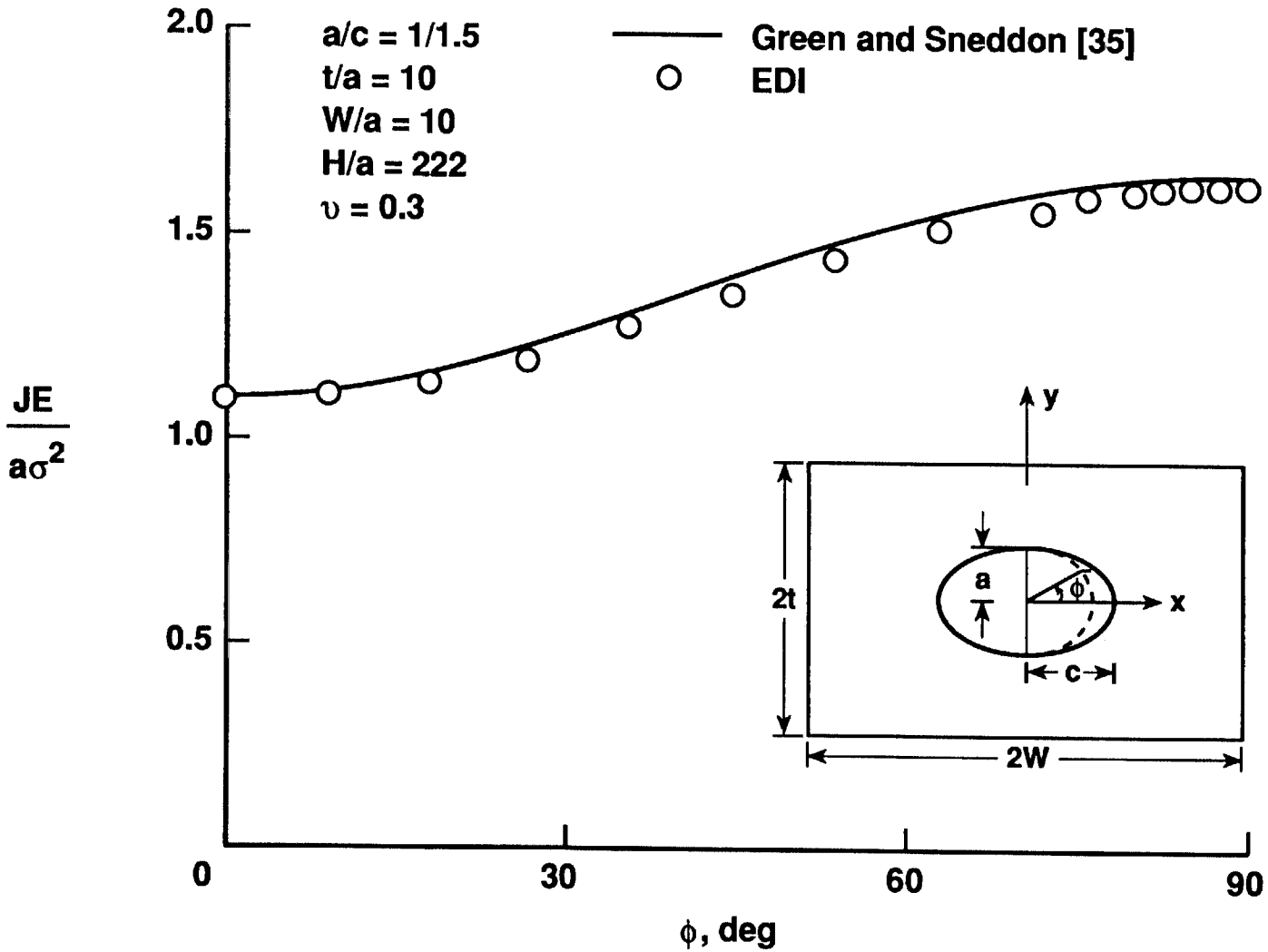

Figure 15. Application of EDI method to 8-node isoparametric element.

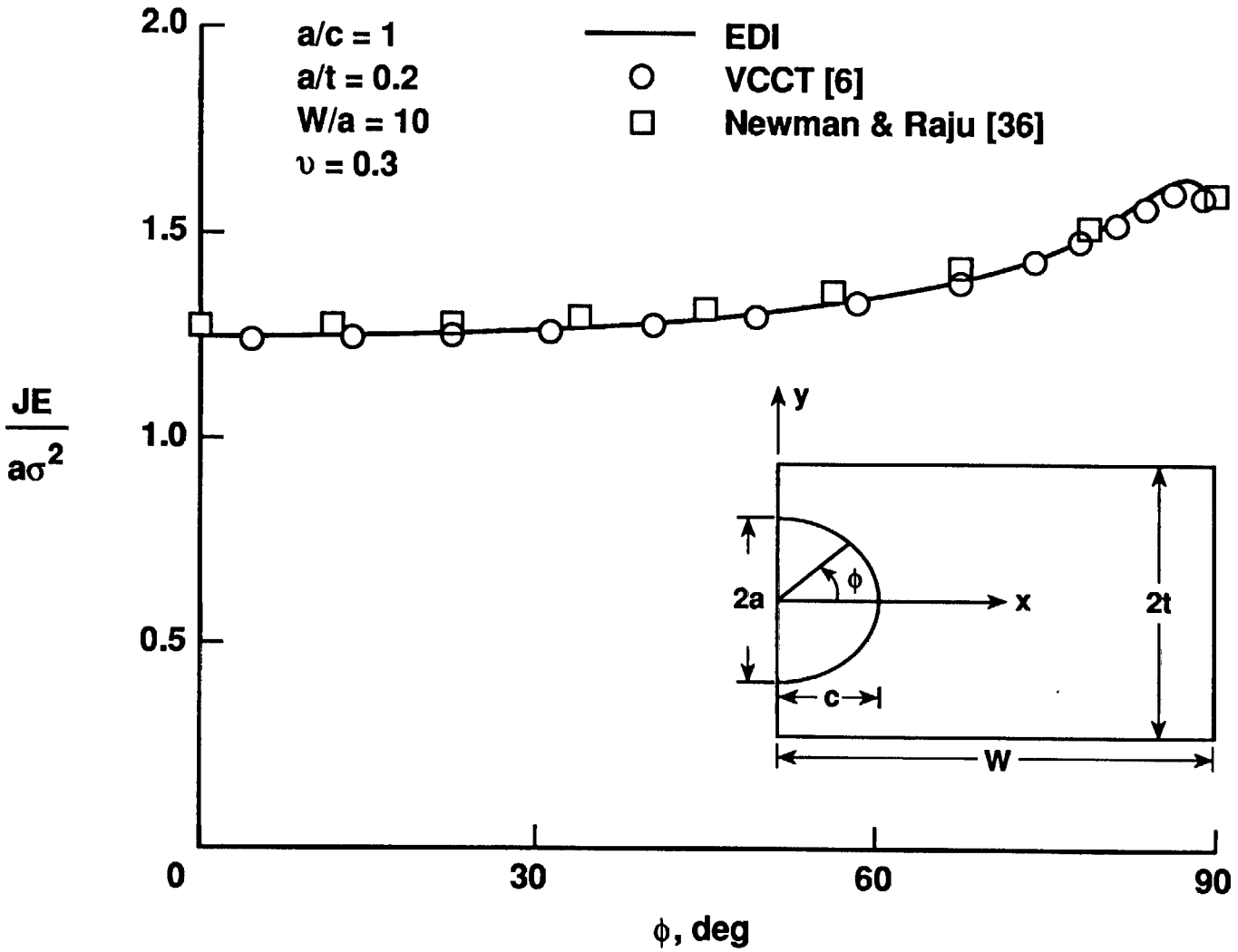

Figure 16. Comparison of normalized J distribution for a semi-circular surface crack from EDI, VCCT, and force methods.

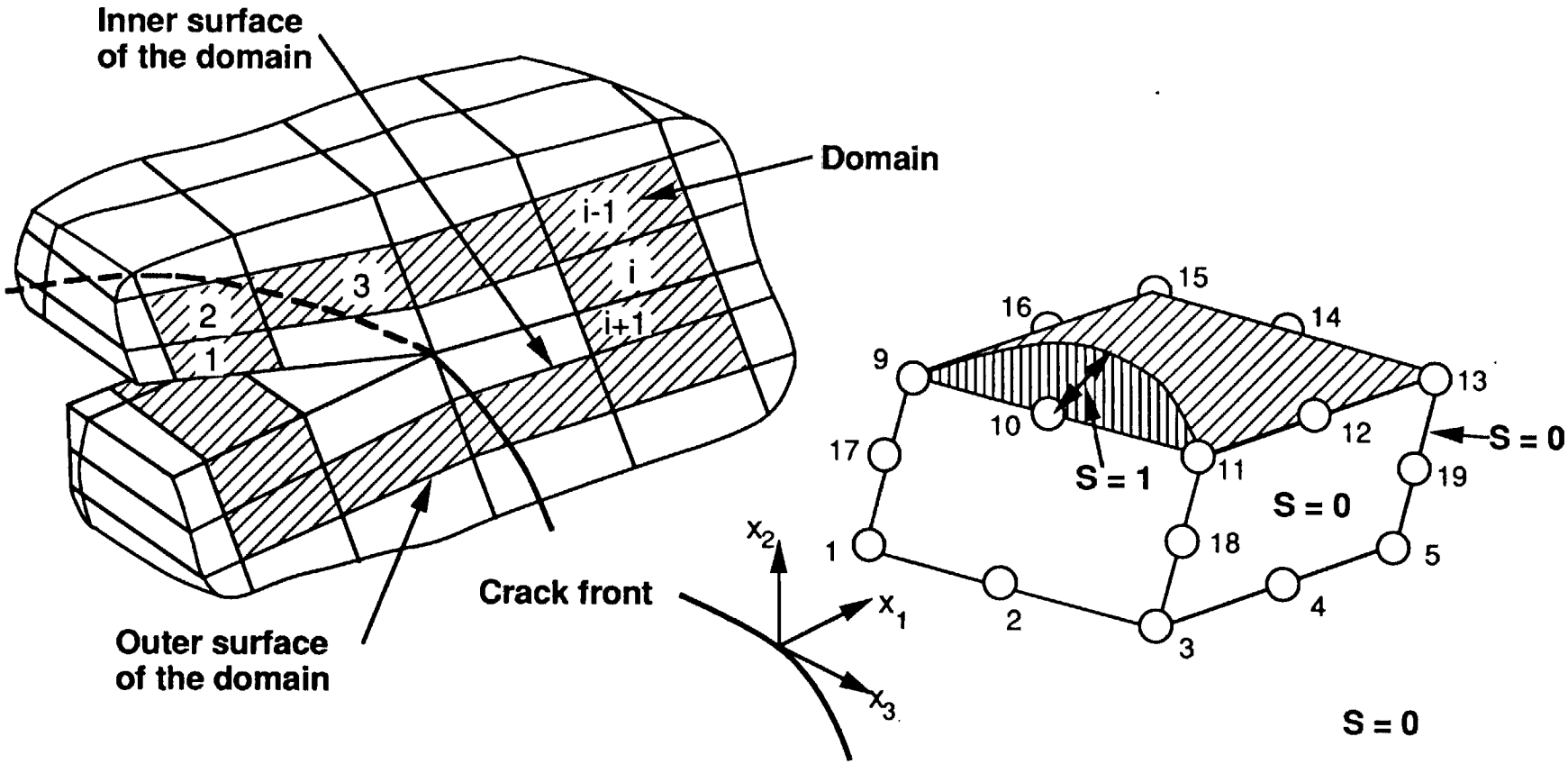

(a) Domain around the crack front

(b) Typical element i and distribution of S-function

Figure 17.- Typical finite-element model and a domain description near the crack front.

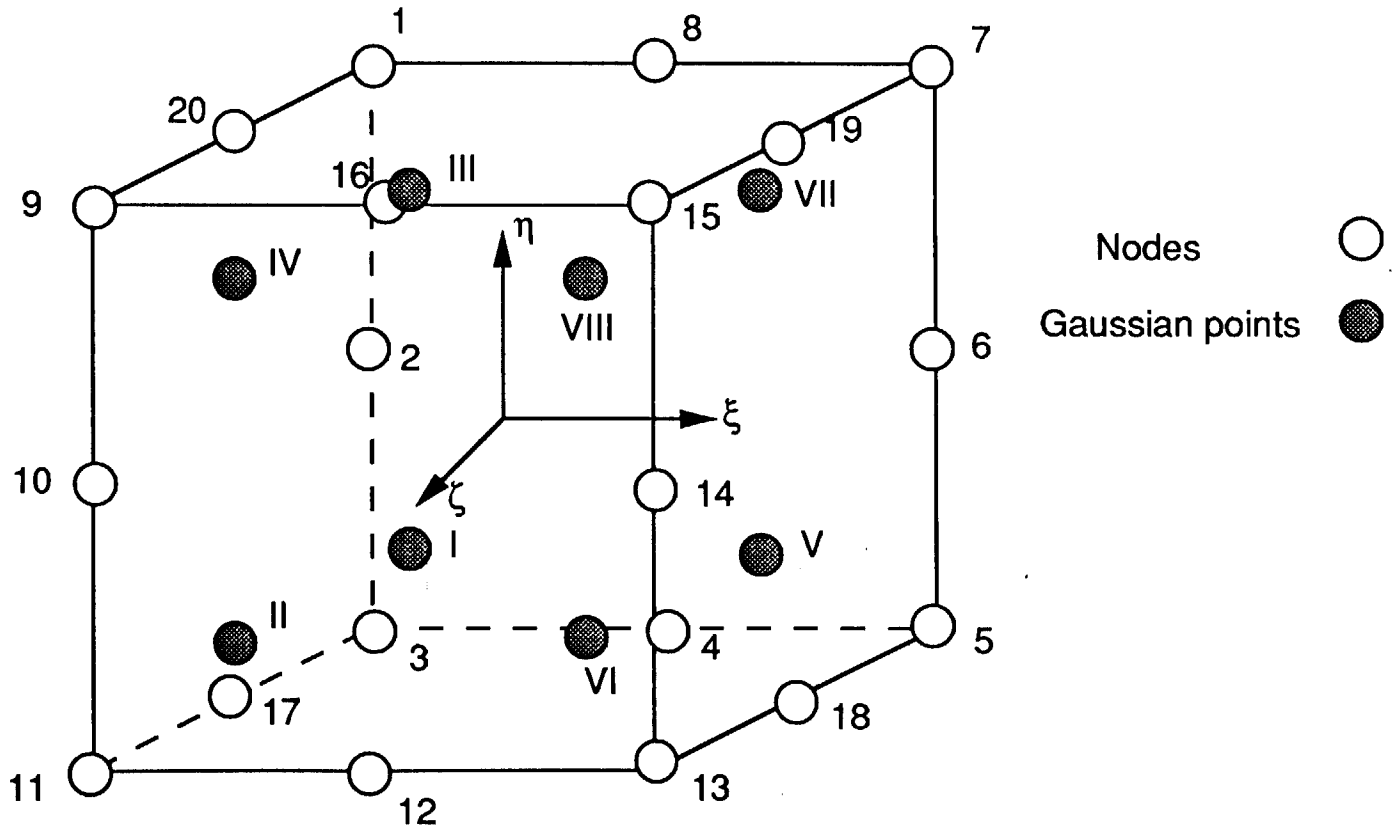

Figure 18.- Nodes and Gaussian quadrature points (2x2x2) in a 20-node isoparametric element.

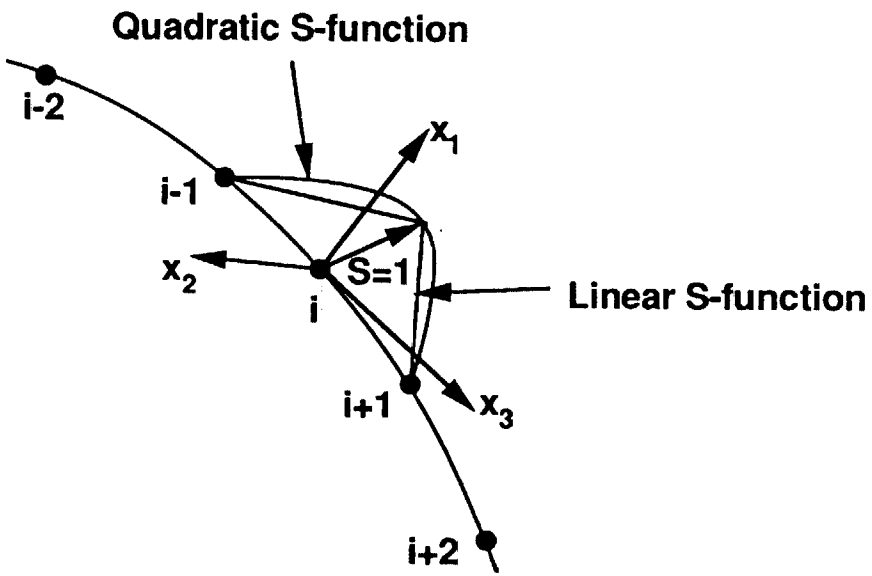

Figure 19.- Descretization of the crack front and linear and quadratic S-function.

NASA
National Aeronautics and Space Administration

Report Documentation Page

1. Report No.	2. Government Accession No.	3. Recipient's Catalog No.
NASA CR-182021		

4. Title and Subtitle	5. Report Date
An Equivalent Domain Integral Method for Three-Dimensional Mixed-Mode Fracture Problems	August 1991
	6. Performing Organization Code

7. Author(s)	8. Performing Organization Report No.
K. N. Shivakumar and I. S. Raju	10. Work Unit No. 505-63-50-04

9. Performing Organization Name and Address	11. Contract or Grant No.
Analytical Services and Materials, Inc. Hampton, VA 23665-5225	NAS1-18599
	13. Type of Report and Period Covered

12. Sponsoring Agency Name and Address	Contractor Report
NASA Langley Research Center Hampton, VA 23665-5225	14. Sponsoring Agency Code

15. Supplementary Notes

Langley Technical Monitor: C. E. Harris

16. Abstract

A general formulation of the equivalent domain integral (EDI) method for mixed-mode fracture problems in cracked solids is presented. The method is discussed in the context of a 3-D finite-element analysis. The J-integral consists of two parts: the volume integral of the crack front potential over a torus enclosing the crack front and the crack surface integral due to the crack front potential plus the crack-face loading. In mixed-mode crack problems the total J-integral is split into J_I, J_{II}, and J_{III} representing the severity of the crack front in three modes of deformations. The direct and decomposition methods are used to separate the modes. These two methods were applied to several mixed-mode fracture problems were analyzed and results found to agree well with those available in the literature. The method lends itself to be used as a post-processing subroutine in a general purpose finite-element program

17. Key Words (Suggested by Author(s))	18. Distribution Statement
Mixed mode fracture Three-Dimensional analysis Crack Equivalent domain integral J-integral Finite-element analysis	Unclassified - Unlimited Subject Category - 39

19. Security Classif. (of this report)	20. Security Classif. (of this page)	21. No. of pages	22. Price
Unclassified	Unclassified	59	A04

NASA FORM 1626 OCT 86